Tectonic controls on the long-term carbon isotope mass balance

Graham A. Shields[1] and Benjamin J. W. Mills[2]

[1]Department of Earth Sciences, University College London, Gower Street, London WC1E 6BT, UK;
g.shields@ucl.ac.uk

[2]School of Earth and Environment, University of Leeds, Leeds LS2 9JT, UK;
b.mills@leeds.ac.uk

Keywords

Author contributions.

G.S. designed the study, B.M. computed numerical results, and both authors contributed to the analysis and writing.

Abstract

The long-term, steady-state marine carbon isotope record reflects changes to the proportional burial rate of organic carbon relative to total carbon on a global scale. For this reason, times of high $\delta^{13}C$ are conventionally interpreted to be oxygenation events caused by excess organic burial. Here we show that the carbon isotope mass balance is also significantly affected by tectonic uplift and erosion via changes to the inorganic carbon cycle that are independent of changes to the isotopic composition of carbon input. This view is supported by inverse co-variance between $\delta^{13}C$ and a range of uplift proxies, including seawater $^{87}Sr/^{86}Sr$, that demonstrates how erosional forcing of carbonate weathering outweighs that of organic burial on geological time scales. A model of the long-term carbon cycle shows that increases in $\delta^{13}C$ need not be associated with increased organic burial and that alternative tectonic drivers (erosion, outgassing) provide testable and plausible explanations for sustained deviations from the long-term $\delta^{13}C$ mean. Our approach emphasizes the commonly overlooked difference between how net and gross carbon fluxes affect the long-term carbon isotope mass balance, and may lead to reassessment of the role that the $\delta^{13}C$ record plays in reconstructing the oxygenation of Earth's surface environment.

Significance

The carbon isotope record has played a major role in reconstructing the oxygen and carbon dioxide content of the ancient atmosphere. However, known oxygenation events are not always reflected in the isotopic record of marine carbonate rocks, while conventional interpretations imply that less organic matter is buried when erosion rates are high, which is hard to explain. Here we show that both issues can be resolved if limestone weathering makes up a proportionately greater fraction of the global carbon cycle at high erosion rates. We argue that the link between carbon isotopes and oxygenation is more tenuous than commonly assumed, and propose a case-by-case re-examination of Earth's oxygenation history.

/body

Introduction

Earth's highly oxygenated atmosphere derives largely from the splitting of the water molecule during photosynthesis. Respiration and decay reverse this process, consuming oxygen, but the burial of organic matter in sediments allows oxygen to accumulate in the atmosphere. Net oxygenation may also arise from burial of reduced sulphur species, but the organic carbon burial flux has been the major source of oxygen throughout the Phanerozoic (1-6).

Because photosynthesis results in ^{13}C-depleted organic carbon, the carbon isotope composition of past oceans has played an important role in tracing the oxygenation of Earth's surface environment. The conventional interpretation of C-isotope mass balance (7) presumes that prolonged intervals of high carbonate $\delta^{13}C$ are the result of elevated rates of organic carbon burial (removing a larger fraction of ^{13}C-depleted organic matter), and so correspond to an excess of oxygen production over consumption, which is in large part due to the oxidation of organic matter during surface weathering. This paradigm has led to the view that atmospheric oxygen levels rose at three crucial junctures in Earth history: at ~2.1 Ga (8-9), ~0.8 Ga (10-11) and ~0.3 Ga (7,12), and this has become generally accepted (13).

This paradigm encounters difficulties. Firstly, although Earth's oxygenation history does not rely solely on carbon isotope data, it is remarkable that independent evidence for oxygenation does not always coincide with high $\delta^{13}C$ (14). The Ediacaran-Cambrian faunal radiation (Cambrian Explosion), which is commonly attributed to oxygenation, is strangely accompanied by low, rather than high $\delta^{13}C$ (Fig. 1), while the many fluctuations in atmospheric oxygen between 15% and 32% that have been identified using the Phanerozoic carbon isotope record (12), lack corroborating evidence (14). Although such inconsistencies are widely acknowledged, alternative explanations to explain global trends in $\delta^{13}C$ are uncommon. One

possibly viable alternative attributes $\delta^{13}C$ fluctuations to the amount of diagenetically precipitated (and isotopically light) carbonate cement worldwide (14-15). Such large changes remain unsubstantiated, while the link to the global carbon cycle must appeal to a sampling bias, wherein a great mass of isotopically light material can be buried (to drive a positive excursion) yet does not lower the bulk isotopic composition of the carbonates which are analyzed. We argue that the preservation of a $\delta^{13}C$ signal that is correlated with other global processes is evidence against such sampling errors, and must be the result of definable system interactions (Fig. 1).

A second problem stems from the driving mechanism for increased organic burial during times of high $\delta^{13}C$. It is widely supposed that higher rates of organic burial are caused by increased nutrient input and/or sedimentation rates through weathering and erosion (5,11,16-17). However, long-term carbon isotope trends exhibit low, not high values during the collisional phases of supercontinent formation, while $\delta^{13}C$ shows an unexpected inverse relationship with erosion proxies, such as seawater $^{87}Sr/^{86}Sr$ and reconstructed sediment masses (Fig. 1, see SI for correlations), best illustrated by the Ediacaran-Ordovician orogenic interval of exceptionally high sedimentary fluxes, which are independently verified by zircon isotope studies (see SI) . The C isotope record implies therefore that erosional forcing of organic burial does not control the long-term C isotope mass balance, and that any such effect may be outweighed by an erosional forcing of carbonate burial.

The long-term carbon isotope mass balance

Figure 2 shows a representation of the long-term carbon cycle, which forms the basis for isotope mass balance calculations (18). Carbon enters the atmosphere/ocean system by four routes: oxidative weathering of fossil carbon (F_{wg}), carbonate weathering (F_{wc}) and

metamorphic degassing of sedimentary organic carbon (F_{mg}) and carbonates (F_{mc}). Carbon leaves the surface pool via burial of organic carbon (F_{bg}) and inorganic carbonates (F_{bc}), with the fraction of total burial leaving via the organic route denoted f_{org}. The dashed lines in figure 2 show an important difference between net (solid lines) and gross (all lines) fluxes in the carbon cycle, which arises because the carbonate weathering-precipitation cycle is a CO_2 neutral process on long time-scales (19) (see SI).

The C-isotope mass balance (eq. 1) is based around the principle that on time scales greater than the residence time of carbon in the ocean (about 10^5 years), the quantity and isotopic composition of carbon entering and exiting the atmosphere-ocean system (A) must be the same (18):

$$\delta^{13}C_{in} = \delta^{13}C_{org}.f_{org} + \delta^{13}C_{carb}\ (1 - f_{org}) \quad (1)$$

Standard calculations then assume that the average isotopic composition of carbon input ($\delta^{13}C_{in}$) is constant and approximately equal to $\delta^{13}C_{mantle}$ or about -6‰ ±1‰. Rearranging equation (1) then allows the proportion of carbon buried as organic matter (f_{org}) to be read directly from the carbonate C isotope record (20). Knowledge of f_{org}, and the total input (≈ output) rate of carbon, F_{total}, then allows the rate of organic carbon burial, and hence oxygen production to be estimated (9,10):

$$F_{bg} = F_{total} \times (\delta^{13}C_{carb} - \delta^{13}C_{in}) / \Delta B \quad (2)$$

Following this reasoning, positive $\delta^{13}C$ excursions are commonly interpreted as organic C burial events, whereby the resultant oxygenation is quantified using the assumptions that total

C throughput and net fluxes (the net carbon flux on geological time scales excludes the carbonate weathering flux) were similar to the present day, and that f_{org} approximates the proportion of outgassed CO_2 (including weathering sources) that is reduced to organic carbon (9,15). For example, the sustained baseline increase of ~5-6‰ during the early Neoproterozoic (11) is interpreted to imply an approximate doubling of organic burial due to increased phytoplankton body size (10) or high sedimentation rates (11). For the ~2.1 Ga Lomagundi Event of high $\delta^{13}C$, the total excess oxygen produced has been estimated at a massive 12-22 times the present inventory of atmospheric oxygen (8,9), with organic burial rates thought to increase by >20 times over the course of the isotope excursion (21).

Such large increases in organic carbon burial are difficult to reconcile with the operation of the long-term carbon cycle. Whilst organics contribute only around 20-25% of gross carbon burial (i.e. $f_{org} \approx 0.20\text{-}0.25$), they constitute more than 50% (19,6) and even as much as 72% (22) of the net carbon sink. Even a doubling of global organic carbon burial over geological timescales would therefore require a massive reorganization of the carbon cycle, alongside a contemporaneous increase in carbon sources through weathering and degassing, due to the impossibility of the other net sink (carbonate deposition following silicate weathering) being reduced below zero.

A physical erosion control on the carbon isotope mass balance

We propose here that long-term variation in f_{org}, and hence $\delta^{13}C$, may sometimes be driven by changes in the inorganic, rather than the organic side of the carbon cycle. Because the carbonate weathering – deposition cycle is CO_2 neutral on time scales relevant to the C-isotope mass balance, increasing the carbonate weathering (and deposition) rates acts to decrease f_{org} without impacting the net carbon fluxes responsible for driving climate. Although this is not the first

155 study to link changes in carbonate weathering to $\delta^{13}C$, for example, it has been shown that a
156 transient increase in carbonate weathering rates would drive an increase in $\delta^{13}C_{in}$ (23), our
157 proposition differs from previous work by highlighting how sustained changes in carbonate
158 deposition rates can alter f_{org} directly.
159
160 Such changes in the inorganic carbon cycle may be brought about by variation in erosion rates,
161 driving step changes in carbonate weathering, and therefore gross carbon throughput. Whilst
162 changes in erosion rate may also initially affect the net fluxes of silicate weathering and organic
163 C burial, these must eventually return to balance the carbon cycle at steady state via temperature
164 and nutrient feedbacks. There is no such requirement for carbonate weathering. This key
165 difference between the net and gross carbon fluxes may explain why the erosional forcing of
166 organic burial does not keep pace with carbonate burial during the early Palaeozoic and other
167 orogenic events (Fig. 1).
168
169
170 Considering that mountains dominate global denudation rates (24), and that carbonate
171 weathering is proportionately more important at higher erosion rates (25), we argue that f_{org}
172 (and hence the $\delta^{13}C$ composition of the atmosphere-ocean system) will be lowered by tectonic
173 uplift and erosion, unless compensated for by increased rates of net carbon flux (outgassing).
174 Conversely, during periods of low denudation rates, $\delta^{13}C$ values will tend to be higher, although
175 the overall weathering flux and organic burial rates may be lower. This is apparent when
176 considering the evidence for low $\delta^{13}C$ during times of supercontinent formation and high $\delta^{13}C$
177 during times of supercontinent stability (16, 26), and can be observed by rearranging equation
178 (2), assuming that erosion affects F_{total}:
179

$$\delta^{13}C_{carb} = (F_{bg} \times \Delta B)/F_{total} + \delta^{13}C_{in} \quad (3)$$

Taking average values from the literature for carbon fluxes ($F_{wg} = 7.75\times10^{12}$ mol/yr, $F_{wc} = 24\times10^{12}$ mol/yr; $F_{mg} = 1.25\ x10^{12}$ mol/yr; $F_{mc} = 8\ x10^{12}$ mol/yr; $F_{bg} = 9x10^{12}$ mol/yr; $F_{total} = F_{wc} + F_{mc} + F_{wg} + F_{mg} = 41\ x10^{12}$ mol/yr (19, 27), equation (3) suggests that trends in the long-term $\delta^{13}C$ average of ~-1‰ to ~+5‰ can be explained by varying the carbonate weathering flux between 1.5 times and 0.2 times the present day rate, respectively, without requiring any change in the rate of organic carbon burial. Such changes are within the limits of published estimates based on the Sr isotope record and/or sedimentation rates (see SI). Note that this mechanism does not require changes in $\delta^{13}C_{in.}$

Modelling the carbon isotope mass balance

To illustrate this idea, we compute the steady states of the long-term carbon cycle model with respect to the relative global erosion rate (Figure 3). The flux calculations follow the GEOCARB and COPSE models (6, 26) under present day conditions, including both direct erosion and temperature effects on weathering fluxes. The isotope mass balance calculations in our model do not differ from those employed in Berner's analysis (5), but critically our model takes into account the effects of erosion on carbonate weathering. This is in line with the above discussion, and with direct evidence for considerable carbonate weathering in areas of high erosion and relief, e.g. the mountainous and foreland areas of the Andes (28). See SI for further model discussion.

An important consideration in this work is that changes in erosion rate also alter the rate of organic carbon burial via changes to the phosphorus cycle. To explore this further we link the rate of organic carbon burial in the model to the availability of phosphorus (22, 6). Phosphorus

205 enters the surface system via the weathering of silicate, carbonate and organic C-bearing rocks,
206 and the strength of the relationship between erosion and organic C burial depends on the P
207 delivery from the weathering of each individual rock type.
208
209 Recent studies of P delivery from different rock types (29, 30) suggest that silicates play the
210 major role, delivering more than 50% of riverine P (see SI). The model run showing this setup
211 (M1) is shown in bold in figure 3. When the weathering of silicates is chiefly responsible for P
212 delivery, an increase in erosion will not greatly affect the steady state P delivery or organic C
213 burial, because the global silicate weathering rate is tightly controlled at steady state by the rate
214 of CO_2 release (which remains constant in the model), and by any imbalance in the organic C
215 cycle.
216
217 Dashed lines in figure 3 show results when silicates are assumed to contribute only ~17% of
218 global P delivery (M2), as was assumed in the original COPSE model, based on crustal
219 inventories rather than supply rates (6). The dotted lines (M3) show a more extreme case where
220 all P delivery results from carbonate weathering. These configurations show that if most P is
221 supplied by the weathering of carbonates, or follows a similar erosional forcing to carbonates
222 (i.e. preferentially weathered at high erosion rates) (25), then an increase in erosion rate would
223 significantly increase P delivery, and therefore organic C burial, at steady state. This would act
224 to counter the direct effect of increased erosion and carbonate weathering/deposition on $\delta^{13}C$,
225 but only as far as carbon mass balance can allow.
226
227 We conclude from this analysis that changes in erosion rates most likely exert a powerful first-
228 order control on long term carbonate $\delta^{13}C$, which is only partially nullified by associated
229 changes in the phosphorus cycle and organic carbon burial.

We acknowledge that the long-term effects of erosion on global P delivery and organic carbon burial are still poorly constrained. Uncertainties exist in the various temperature and erosion effects on individual chemical weathering fluxes, the degree of preferential chemical weathering of accessory apatite minerals, and the possibility that changes in sedimentation rate may impact organic carbon burial differently to the burial of carbonates. In particular, it has been proposed that increased rates of sedimentation will enhance the preservation of buried organic carbon and phosphorus (5). Our model calculates the rate of organic carbon burial based on a relationship between ocean phosphate, new production and sedimentation rate (31), but we have also run an alternative model setup to further explore this idea, wherein we strengthen this relationship by giving the burial rates of organic carbon and phosphorus an additional linear dependence on the global erosion rate. The model results for ocean phosphate concentration are altered under these assumptions, but the steady-state burial rates of carbon and phosphorus are not affected, as they are ultimately constrained by the supply flux of P from weathering (see SI for more details).

Our model run M1 shows what we consider to be the current best guess for these mechanisms (see SI for more details and other model runs), but a model is not unequivocal proof, and it is clearly theoretically possible for erosion to increase organic C burial more than it increases the burial rate of carbonates (e.g. model run M3). However, if this were the case we would expect $\delta^{13}C$ values to increase with increasing erosion rates, but this is effectively falsified by the anti-correlation of $\delta^{13}C$ and all available erosion proxies. We therefore conclude that although erosion rates must certainly increase the rate of P delivery and organic C burial, such increases must be less than the increases to the burial rate of carbonates.

Figure 4 shows a series of time-dependent model runs where a +3‰ positive excursion in $\delta^{13}C$ is caused by either increasing organic carbon burial (via increased P delivery), or decreasing the erosion rate. Increasing $\delta^{13}C$ via an organic C burial event (Figure 4. A-E) results in a decrease in the atmosphere/ocean carbon reservoir, i.e. a decrease in atmospheric pCO_2, and global cooling. Driving a similar positive excursion via a reduction in erosion rates (Figure 4. F-J) causes a warming event due to the weakening of silicate weathering. Importantly, we show that a positive $\delta^{13}C$ excursion may be coincident with either an increase, or decrease in the rate of organic carbon burial. This should be a serious consideration for work aiming to tie the C isotope record to global biogeochemical events.

An important factor influencing the time-dependent response of the model is the assumption of 'rapid recycling' of isotope signals due to the predominant weathering of recently-deposited sediments. This idea has been explored in early carbon and sulphur cycle models (7), and is included in the GEOCARB models (5). We include this effect here by reducing the size of the crustal pools of organic carbon and carbonates to around 10% of the total crustal inventory, allowing for much quicker variation in isotopic composition (RR on, solid lines in figure 4). This follows Berner (5, 7). Dashed lines assume no rapid recycling, i.e. that the isotopic signature of weathered material represents the whole crustal inventory. As may be expected, the rapid recycling model acquires steady state around an order of magnitude quicker than the non-RR model. However, the choice of models does not affect the qualitative dynamics we wish to demonstrate.

The isotopic composition of carbon inputs ($\delta^{13}C_{in}$) is not fixed in our model, but responds to the changing composition of the crustal reservoirs. Although changes to $\delta^{13}C_{in}$ (e.g. due to preferential weathering of high-$\delta^{13}C$ lithologies) have been shown to drive C isotope

excursions (20, 23), the mechanism explored in this paper does not depend on variations in $\delta^{13}C_{in}$. As an example we run the model with this parameter fixed (Figure S7), which shows the same qualitative results.

Interrogating carbon isotope excursions

A positive carbon isotope excursion caused by changes to the inorganic carbon cycle has different climatic effects from one caused by increasing the burial rate of organics: notably an increase in CO_2 and surface temperature, rather than a decrease. Such testable distinctions allow us to constrain the causes of specific carbon isotope events, and suggest that major, but short-lived $\delta^{13}C$ events, which coincide with global cooling, such as the late Ordovician Hirnantian event, could potentially relate to excess organic burial. The longer Permo-Carboniferous glaciations also occurred at a time of generally high $\delta^{13}C$, and are thus consistent with an elevated organic burial flux, perhaps associated with the evolution of a modern land biota (32). However, relatively low erosion rates throughout this period imply that rates of organic C burial need not have been as high as previously thought – potentially resolving conflicts over the prediction of hyperambient O_2 levels (5). By contrast, glaciation during the Cenozoic is associated with decreasing $\delta^{13}C$, and so appears to be more consistent with the notion that the erosional forcing of carbonate deposition outweighed that of organic burial.

Some times of elevated $\delta^{13}C$ do not coincide with glaciation, and this is the case for the post-glacial Lomagundi Event of exceptionally high $\delta^{13}C$ during the Palaeoproterozoic . Such high $\delta^{13}C$ values may result from a hugely increased oxidative weathering flux (21), following the Great Oxidation Event, which could have been self-sustained by oxygenic siderite (iron carbonate) weathering (22). Although not related to decreased erosion rates, the Lomagundi Event can still be viewed as a time of proportionately higher net carbon flux relative to gross

carbon throughput, in the same way as we argue for other times of high baseline $\delta^{13}C$, such as during the Tonian Period of supercontinent peneplanation. Note that in none of these cases does high $\delta^{13}C$ imply net oxygenation. Previously, these well-established $\delta^{13}C$ events were first-order determinants in our understanding of Earth's oxygenation history.

Despite our emphasis here on erosional controls on $\delta^{13}C$, we view the carbon isotope mass balance as a proportional parameter, whereby changes to the long-term norm correspond to changes in the proportion that carbonate weathering makes up of the global carbon cycle. In this regard, the anti-correlation between $\delta^{13}C$ and $^{87}Sr/^{86}Sr$ over the past billion years could reflect the dependence of both these parameters on the competing tectonic influences of volcanism versus uplift, rather than erosion *per se*.

Conclusions

The carbon isotope record is most commonly viewed in terms of changing organic carbon burial rates, and less in terms of the proportional organic component of the carbon cycle. By viewing $\delta^{13}C$ as a combination of net and gross carbon fluxes (and removing the common assumption that carbonate / silicate / organic weathering systematics are invariantly proportional), we show that higher proportional organic burial (higher f_{org}) can result from a decreased global weathering (carbonate) flux to the ocean and may not be driven directly by changes in the organic carbon burial flux. Moreover, it appears that tectonic controls may plausibly be the underlying drivers of carbon isotope trends that were previously attributed either to organic carbon burial or to the changing isotopic composition of carbon sources. This is evidenced by the anti-correlation between carbonate $\delta^{13}C$ and erosion proxies such as $^{87}Sr/^{86}Sr$ and reconstructed sediment abundance. There seems to be no systematic relationship between $\delta^{13}C$ and oxygenation through carbon burial, and we suggest therefore that the

oxygenation history of the Earth be reassessed on a case-by-case basis in order to better take into account the distinction between net and gross fluxes.

References

1. Kump LR., Garrels RM (1986) Modeling Atmospheric O_2 in the Global Sedimentary Redox Cycle. *American Journal of Science* 286: 337-360.
2. Bottrell SH, Newton, RJ (2006) Reconstruction of changes in global sulfur cycling from marine sulfate isotopes. *Earth Science Reviews* 75: 59-83.
3. Smith RW, Bianchi TS, Allison M, Savage C, Galy V (2015) High rates of organic carbon burial in fjord sediments globally. *Nat Geosci* 8: 450-453.
4. Berner RA, Canfield DE (1989) A new model for atmospheric oxygen over Phanerozoic time. *Amer J Sci* 289: 333-361.
5. Berner RA (2006) GEOCARBSULF: A combined model for Phanerozoic atmospheric O_2 and CO_2. *Geochim et Cosmochim Acta* 70: 5653-5664.
6. Bergman NM, Lenton TM, Watson AJ (2004) COPSE: A new model of biogeochemical cycling over Phanerozoic time. *Amer J Sci* 304: 397-437.
7. Berner RA (1987) Models for carbon and sulfur cycles and atmospheric oxygen: application to Paleozoic geologic history. *Amer J Sci* 287: 177-196.
8. Karhu JA, Holland HD (1996) Carbon isotopes and the rise of atmospheric oxygen. *Geology* 24: 867-870.
9. Holland HD (2002) Volcanic gases, black smokers, and the Great Oxidation Event. *Geochim et Cosmochim Acta* 66: 3811-3826.
10. Knoll AH, Hayes JM, Kaufman AJ, Swett K, Lambert IB (1986) Secular variations in carbon isotope ratios from Upper Proterozoic successions of Svalbard and East Greenland. *Nature* 321: 832-838.

11. Des Marais DJ, Strauss H, Summons RE, Hayes JM (1992) Carbon isotope evidence for the stepwise oxidation of the Proterozoic environment. *Nature* 359: 605-609.
12. Berner RA (2009) Phanerozoic atmospheric oxygen: new results using the GEOCARBSULF model. *Amer J Sci* 309: 603-606.
13. Lyons TW, Reinhard CT, Planavsky NJ (2014) The rise of oxygen in Earth's ocean and atmosphere. *Nature* 506: 307-315.
14. Schrag DP, Higgins JA, Macdonald FA, Johnston DT (2013) Authigenic Carbonate and the History of the Global Carbon Cycle. *Science* 339: 540-543.
15. Hayes JM, Waldbauer JR (2006) The carbon cycle and associated redox processes through time. *Phil. Trans. R. Soc. B* 361: 931-950.
16. Campbell IH, Allen CM (2008) Formation of supercontinents linked to increases in atmospheric oxygen. *Nat Geosci* 1: 554-558.
17. Galy V, Peucker-Ehrenbrink B, Eglinton T (2015) Global carbon export from the terrestrial biosphere controlled by erosion. *Nature* 521: 204-207.
18. Garrels RM, Lerman A (1984) Coupling the sedimentary sulfur and carbon cycles - an improved model. *Amer J Sci* 284: 989-1007.
19. Berner RA (1991) A model for atmospheric CO_2 over Phanerozoic time. *Amer J Sci* 291: 339-376.
20. Kump LR, Arthur MA (1999) Interpreting carbon-isotope excursions: carbonates and organic matter. *Chem Geol* 161: 181-198.
21. Bekker A, Holland HD (2012) Oxygen overshoot and recovery during the early Paleoproterozoic. *EPSL* 317-318: 295-304.
22. Bachan A, Kump LR (2015) The rise of oxygen and siderite oxidation during the Lomagundi Event. *Proc Natl Acad Sci USA* 112: 6562-6567.

379 23. Kump LR et al (1999) A weathering hypothesis for glaciation at high atmospheric pCO_2
380 during the late Ordovician. *Palaeogeog, Palaeoclimat, Palaeoecol* 152: 173-187.
381 24. Larsen IJ, Montgomery DR, Greenberg HM (2014) The contribution of mountains to
382 global denudation. *Geology* 42: 527-530.
383 25. Jacobson AD, Blum JD (2003) Relationship between mechanical erosion and atmospheric
384 CO_2 consumption in the New Zealand Southern Alps. *Geology* 31: 865-868.
385 26. Berner RA (1994) Geocarb II: A revised model of atmospheric CO_2 over Phanerozoic
386 time. *Amer J Sci* 294: 56-91.
387 27. Kasting JF (2013) What caused the rise of atmospheric O_2? *Chem Geol* 362: 13-25.
388 28. Moquet J-S, et al (2011) Chemical weathering and atmospheric/soil CO_2 uptake in the
389 Andean and Foreland Amazon basins. *Chem Geol* 287: 1-26.
390 29. Hartmann J, Moosdorf N, Lauerwald R, Hinderer M, West AJ (2014) Global chemical
391 weathering and associated P-release – The role of lithology, temperature and soil properties
392 *Chem Geol* 363: 145-163.
393 30. Compton J, et al (2000) Variations in the global phosphorus cycle. In *Marine*
394 *Authigenesis: From Global to Microbial*, SEPM Special Publication 66: 21-33.
395 31. Van Cappellen P, Ingall ED (1994) Benthic phosphorus regeneration, net primary
396 production, and ocean anoxia – a model of the coupled marine biogeochemical cycles of
397 carbon and phosphorus *Paleoceanography* 9: 677-692.
398 32. Lenton TM et al (2016) Earliest land plants created modern levels of atmospheric oxygen.
399 *Proc Natl Acad Sci USA* 113(35): 9704-9709.
400 33. Gradstein FM, Ogg JG, Schmitz MD, Ogg GM (Eds) *The Geologic Time Scale 2012:*
401 *volume 1*. Elsevier, 435pp.

34. Hay WW et al (2006) Evaporites and the salinity of the ocean during the Phanerozoic: Implications for climate, ocean circulation and life. *Palaeogeog, Palaeoclimat, Palaeoecol* 240: 3-46.

35. Hayes JM, Strauss H, Kaufman AJ (1999) The abundance of ^{13}C in marine organic matter and isotopic fractionation in the global biogeochemical cycle of carbon during the past 800 Ma. *Chem Geol* 161: 103-125.

36. Veizer J (1985) Carbonates and ancient oceans: isotopic and chemical record on time scales of $10^7 – 10^8$ years. In: The carbon cycle and atmospheric CO_2: Natural variations, Archean to Present. Eds: E.T. Sundquist, W.S. Broeker. *AGU Geophysical Monograph* 32: 595-601.

37. Worsley TR, Moody JB, Nance RD (1985) Proterozoic to Recent tectonic tuning of biogeochemical cycles. In: The carbon cycle and atmospheric CO_2: Natural variations, Archean to Present. Eds: E.T. Sundquist, W.S. Broecker. *AGU Geophysical Monograph* 32: 561-572.

38. Rothman DH (2002) Atmospheric carbon dioxide levels for the last 500 million years. *Proc Natl Acad Sci USA* 99: 4167-4171.

39. Brasier MD, Lindsay JF (2001) Did supercontinent amalgamation trigger the “Cambrian Explosion”? In: The ecology of the Cambrian radiation. Eds: A.Y. Zhuravlev, R. Riding. Columbia University Press, New York, pp. 69-89.

40. Squire RJ, Campbell IH, Allen CM, Wilson CJL (2006) Did the Transgondwanan supermountain trigger the explosive radiation of animals on Earth? *EPSL* 250: 116-133.

41. Bradley DC (2011) Secular trends in the geologic record and the supercontinent cycle. *Earth Sci Rev* 108: 16-33.

42. Peters SE, Gaines RR (2012) Formation of the ‘Great Unconformity’ as a trigger for the Cambrian explosion. *Nature* 484: 363-366.

427 43. Spencer CJ et al (2014) Proterozoic onset of crustal reworking and collisional tectonics:
428 Reappraisal of the zircon oxygen isotope record. *Geology* 42: 451-454.
429 44. Berner RA (2004), The Phanerozoic Carbon Cycle: CO_2 and O_2, Oxford Univ. Press, New
430 York, USA.
431 45. Dilek Y, Furnes H (2011) Ophiolite genesis and global tectonics: Geochemical and
432 tectonic fingerprinting of ancient oceanic lithosphere. *GSA Bulletin* 123: 387-411.
433 46. Condie K (2011) Earth as an evolving planetary system. *Elsevier Academic Press.*
434 Cambridge MA, USA.
435 47. Scotese CR (2001) Atlas of Earth History. *PALEOMAP project*. Arlington, TX, USA.
436 48. Cawood PA, Hawkesworth CJ, Dhuime B (2013) The continental record and the
437 generation of continental crust. *GSA Bulletin* 125: 14-32.
438 49. Krissansen-Totton J, Buick R, Catling DC (2015) A statistical analysis of the carbon
439 isotope record from the Archean to the Phanerozoic and implications for the rise of oxygen.
440 *Amer J Sci* 315: 275-316.
441 50. Sleep NH, Zahnle K (2001) Carbon dioxide cycling and implications for climate on
442 ancient Earth. *J Geophys Res* 106: 1373-1399.
443 51. Royer DL, Donnadieu Y, Park J, Kowalczyk J, Godderis Y (2014) Error analysis of CO_2
444 and O_2 estimates from the long-term geochemical model GEOCARBSULF. *Amer J Sci* 314:
445 1259-1283.
446 52. Mills B, Watson AJ, Goldblatt C, Boyle R, Lenton TM (2011) Timing of Neoproterozoic
447 glaciations linked to transport-limited global weathering. *Nat Geosci* 4: 861-864.
448 53. Li G, Elderfield H (2013) Evolution of carbon cycle over the past 100 million years.
449 *Geochim Cosmochim Acta* 103: 11-25.
450 54. Lenton TM, Watson AJ (2000) Redfield Revisited: 1) Regulation of nitrate, phosphate
451 and oxygen in the ocean. *Global Biogeochemical Cycles* 14: 225-248.

55. Hartmann J, Dürr HH, Moosdorf N, Meybeck M, Kempe S (2012) The geochemical composition of the terrestrial surface (without soils) and comparison with the upper continental crust. *Int J Earth Sci* 101(1): 365-376.

56.Caldeira K, Kasting JF (1992) The life span of the biosphere revisited. *Nature* 360: 721-723.

57. Shields GA (2007) A normalised seawater strontium isotope curve: possible implications for Neoproterozoic-Cambrian weathering rates and the further oxygenation of the Earth. *eEarth* 2: 35-42.

Acknowledgements

G.S.'s contribution was initiated at the WWU (Westfälische Wilhelms-Universität, Münster) during a stay as an Alexander von Humboldt research fellow from 2006-2008. His research was additionally supported by NERC grant NE/I00596X/1 and by a Chinese Academy of Sciences senior visiting researcher fellowship. B.M.'s contribution was supported by the Leverhulme Trust (RPG-2013-106) and a Leeds University Academic Fellowship. C-isotope data were kindly provided by Matthew Saltzman (see ref 33) and shown as a 20 point moving average of 1 Myr bins over the Phanerozoic (Fig. 1).

Figure legends

Fig. 1. Phanerozoic records of marine carbonate $\delta^{13}C$ (33), seawater Sr isotope composition (33) and mass of sedimentary material (two shades correspond to measured and estimated total mass, respectively) (34). Diverse tectonic proxies identify the Ediacaran-Ordovician interval as a time of maximal uplift and erosion, but minimal $\delta^{13}C$ (see SI).

Fig. 2. Long term carbon cycle showing isotope fractionation. A is atmosphere and ocean carbon, G is buried organic carbon and C is buried carbonate carbon. F_b refers to burial fluxes, F_w to weathering and F_m to metamorphic/degassing fluxes. δ_x denotes the isotopic fractionation of reservoir X, and ΔB is the fractionation effect applied to buried organic carbon, taken to represent an average value over the Phanerozoic (35). *Sil* and *Carb* show alkalinity fluxes from silicate and carbonate weathering, respectively, which are combined to calculate F_{bc} (see SI). Dashed lines denote the 'null' carbonate weathering – deposition cycle.

Fig. 3. Steady states of the long-term carbon cycle model. The system shown in Figure 2 is run to steady state for different values of the relative global uplift/erosion rate. Bold lines (M1) show results when silicate weathering delivers around 58% of ocean phosphate (29, see SI), dashed lines (M2) show results when when silicate weathering delivers only 17% of ocean phosphate (6), and dotted lines (M3) show results when all P delivery is instead from carbonate weathering. The equations governing the response of fluxes to reservoir sizes and global temperature follow current models (6, 26). See SI for full model description, MATLAB code, and further evaluation.

Fig. 4. Comparison of positive $\delta^{13}C$ excursions driven by burial and erosion events. Panels show A: Relative model forcing factor. B, Burial fluxes for carbonate (F_{bc}, blue) and organic carbon (F_{bg}, red). C, Ocean phosphate. D, Atmosphere and ocean carbon. E, $\delta^{13}C$ of atmosphere/ocean carbon reservoir. Panels F-J repeat these quantities for the second model scenario. A positive $\delta^{13}C$ excursion is driven by increased organic carbon burial, via enhancement of phosphorus weathering (A-E), and is compared to a positive $\delta^{13}C$ excursion driven by a change in erosion (F-J). Both forcings (green lines) are ramped over a 10 Myr period, beginning at t=0. Solid lines show rapid recycling model (RR on, see text), dashed lines show no rapid recycling. Note that the positive excursion driven by organic C burial is associated with a decrease in atmosphere/ocean carbon (panel D), whilst the excursion driven by erosion is associated with an increase in the carbon reservoir (panel I). P input from weathering follows Hartmann et al. (2014) (29). Full model output is included in the SI.

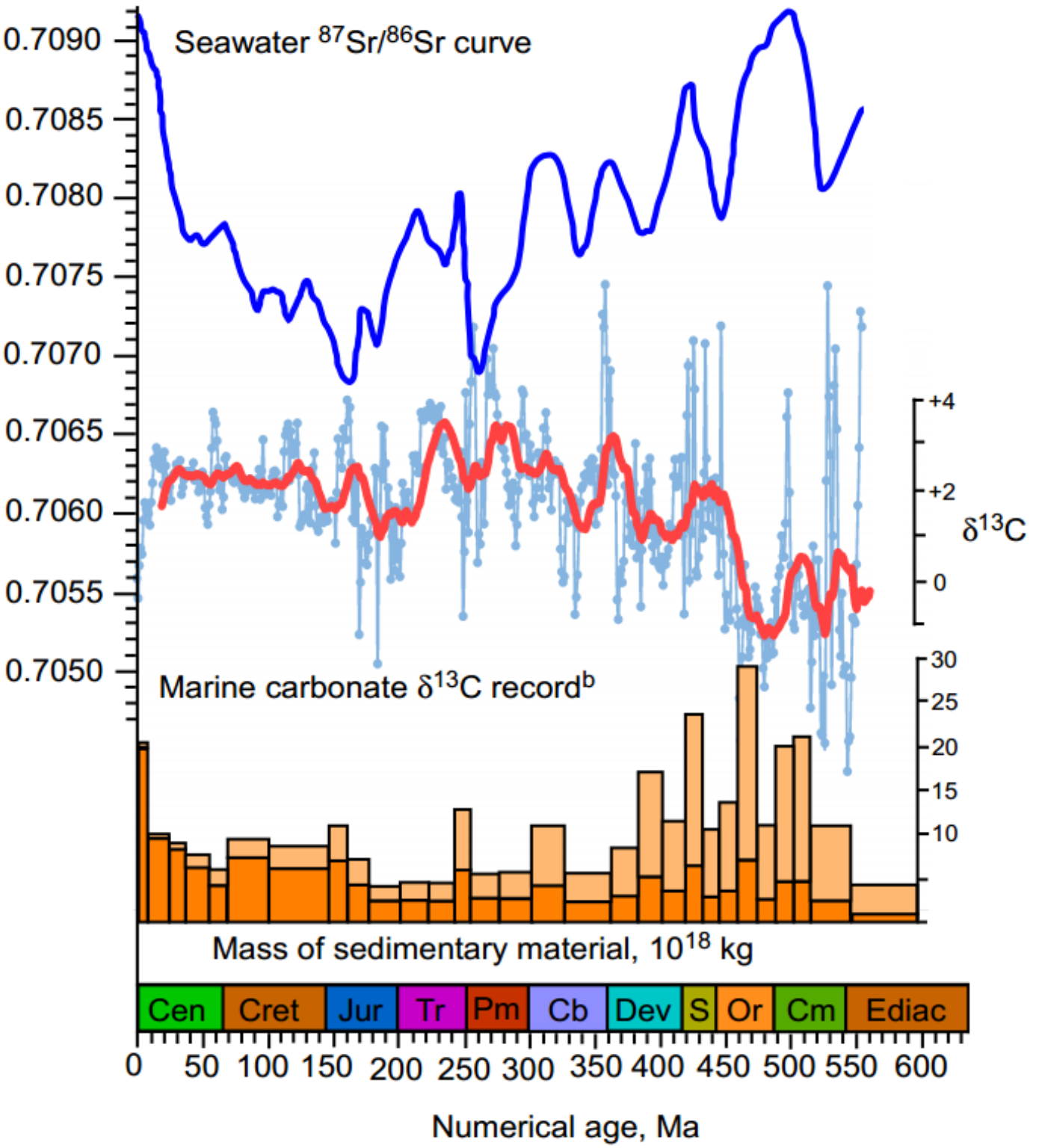
Seawater $^{87}Sr/^{86}Sr$ curve
0.7090
0.7085
0.7080
0.7075
0.7070
0.7065
0.7060
0.7055
0.7050
+4
+2
0
$\delta^{13}C$
Marine carbonate $\delta^{13}C$ record[b]
30
25
20
15
10
Mass of sedimentary material, 10^{18} kg
Cen
Cret
Jur
Tr
Pm
Cb
Dev
S
Or
Cm
Ediac
0 50 100 150 200 250 300 350 400 450 500 550 600
Numerical age, Ma

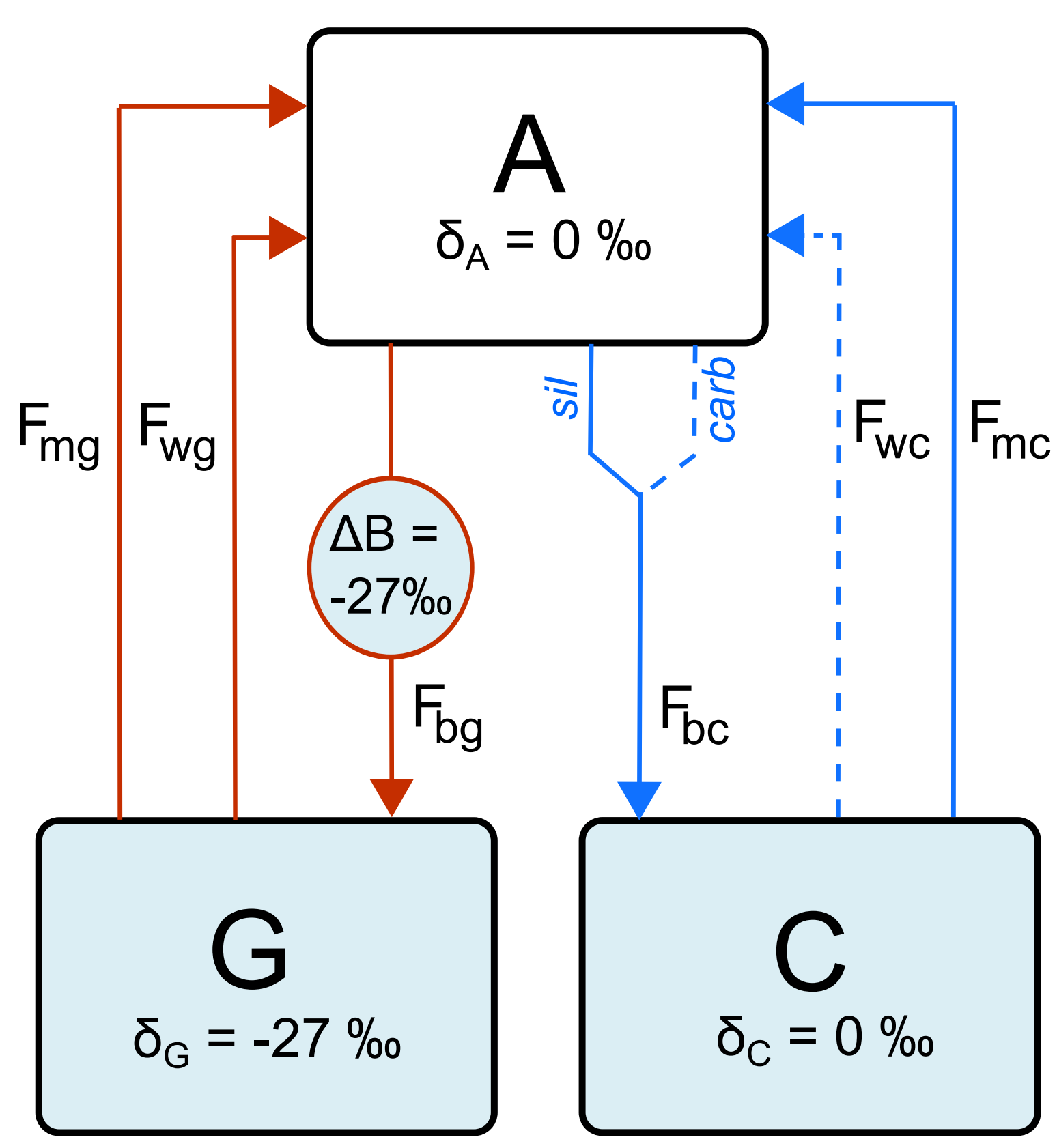
A
δ_A = 0 ‰
F_{mg}
F_{wg}
F_{wc}
F_{mc}
sil
carb
ΔB =
-27‰
F_{bg}
F_{bc}
G
δ_G = -27 ‰
C
δ_C = 0 ‰

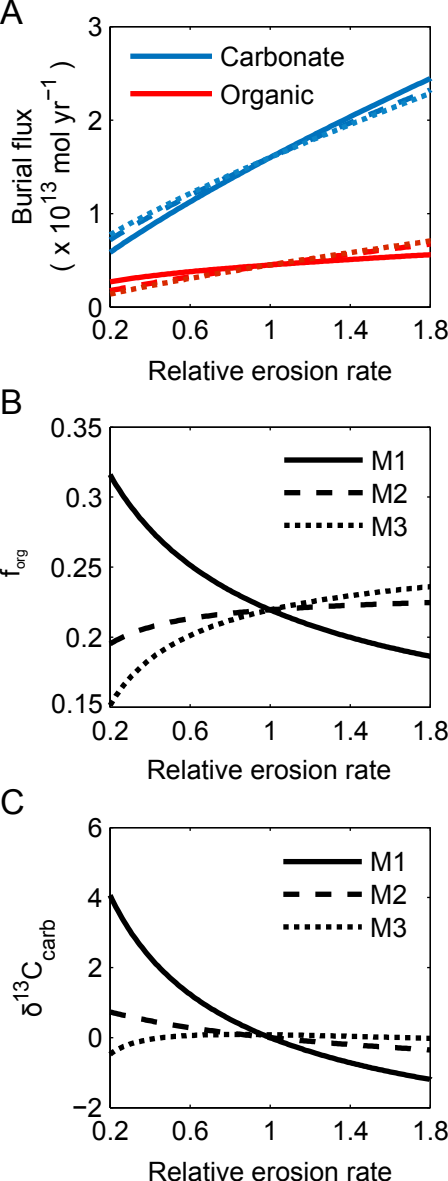
A
Carbonate
Organic
Burial flux
(x 10^13 mol yr^-1)
3
2
1
0
0.2
0.6
1
1.4
1.8
Relative erosion rate
B
M1
M2
M3
f_org
0.35
0.3
0.25
0.2
0.15
0.2
0.6
1
1.4
1.8
Relative erosion rate
C
M1
M2
M3
δ13C_carb
6
4
2
0
−2
0.2
0.6
1
1.4
1.8
Relative erosion rate

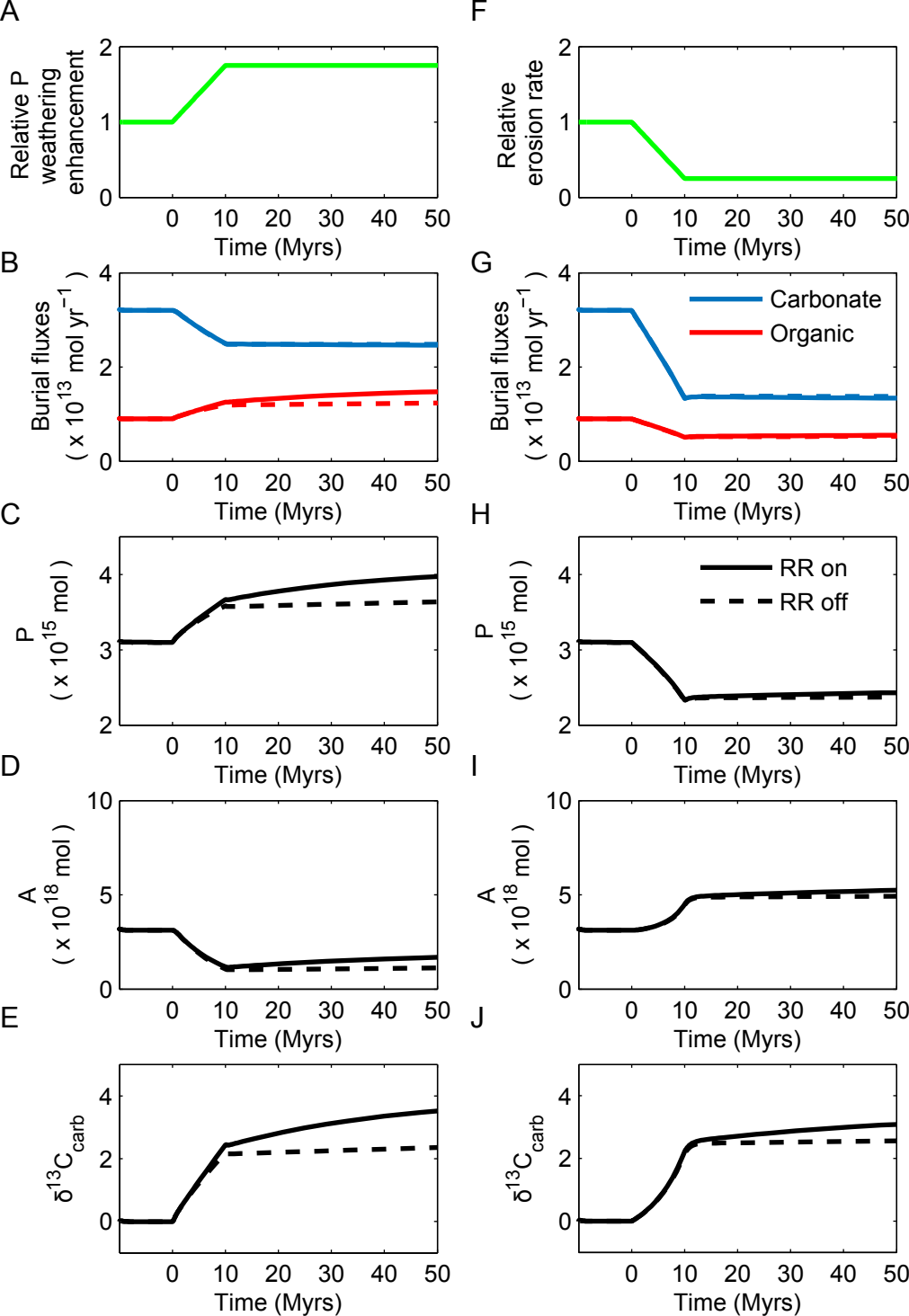
A
Relative P weathering enhancement
Time (Myrs)
B
Burial fluxes (x 10^13 mol yr^-1)
Carbonate
Organic
C
P (x 10^15 mol)
RR on
RR off
D
A (x 10^18 mol)
E
δ13Ccarb
F
Relative erosion rate
G
H
I
J

Supporting Information

SI Materials and Methods

Co-variation of erosion rates and carbonate $\delta^{13}C$.

Inverse correlation between carbonate $\delta^{13}C$ and seawater $^{87}Sr/^{86}Sr$ ratios has been noted in previous studies (36-38), and similar correlations with the reconstructed rate of sediment deposition (34) and the 'relative uplift/erosion' parameter from long term carbon cycle models (5, 6) can be observed using scatter plots (Figure S1). Computing the Pearson product moment correlation coefficient (PMCC) for these datasets gives values of ~-0.5 to -0.4, and fitting a linear regression model (red lines in Figure S1) to the data results in a negative slope, with R^2 values between 0.17 and 0.25. Together, these tests confirm a weak but observable negative correlation in all cases. Efforts to remove the sedimentary recycling 'memory flux' from the $^{87}Sr/^{86}Sr$ record have resulted in an improved correlation with $\delta^{13}C$ (38). We do not expect a strong correlation between erosion proxies and $\delta^{13}C$ due in part to heterogeneities in both datasets, driven by the spatial nature of paleoenvironments, and by sampling and preservation errors. But more importantly, erosion is not the only driving force behind C isotope variation: the argument in this paper is that erosion, via the changing proportion that carbonate weathering makes of total carbon throughput, acts as a base-level control over ~100 Myr time scales, which is supported by the correlations we show here.

Reconstructing paleo-erosion fluxes is difficult, and each method has its own caveats: Sr isotope ratios are controlled by the age and distribution of weathered material, which is undoubtedly influenced by erosion, but has other drivers. Similarly, the observed abundances of sedimentary rocks are subject to preservation and sampling bias. However, over ~100 Myr time scales, the Wilson cycle of supercontinent formation and break-up is widely accepted to

have led to a prolonged period of mountain uplift during the Late Precambrian and early Paleozoic (39-42), followed by a time of supercontinent stability and low erosion rates during the late Paleozoic and Early Mesozoic (43). The relative erosion rate used to drive long-term carbon cycle models (e.g. GEOCARBSULF (5), Figure S1 B) uses a quadratic curve to represent Phanerozoic erosion, analogous to the Wilson cycle and the long-term average variation in sediment mass and Sr isotope ratios (44).

This long-term dynamic is independently evidenced by records of orogenies, collisions and paleogeographies (45-48), and has recently been elucidated by the study of zircon hafnium and oxygen isotope compositions. Zircon εHf and $\delta^{18}O$ values (48, 43) highlight the Ediacaran-Cambrian interval of low carbonate $\delta^{13}C$ as a time of exceptional uplift (unroofing) of deep crustal roots and of sediment reworking, respectively, providing independent and quantitative support for the Wilson cycle dynamic (Figure S2). Consistent with this interpretation, the earlier 'Tonian' interval of exceptionally high $\delta^{13}C$ (10,11) is interpreted as a time of relative tectonic quiescence (48): This peak in carbonate f_{org}, confirmed most recently by Krissansen-Totton et al. (49), occurred during the initial rifting phase of the greatly denuded supercontinent Rodinia (Fig. S2). We conclude that despite the difficulty in reconstructing variation in past erosion rates, the established long-term cyclic changes over the Phanerozoic show a marked inverse correlation with average $\delta^{13}C$ since 500 Ma, and possibly earlier.

Net and gross fluxes in the long-term carbon cycle

The representation of the long term carbon cycle, which forms the basis for isotope mass balance calculations (1, 7, 8) (ms Figure 2), considers changes in the following fluxes: carbon inputs to the surface system via oxidative weathering of fossil carbon (F_{wg}), carbonate weathering (F_{wc}), metamorphic degassing of sedimentary organic carbon (F_{mg}), and degassing

of carbonates (F_{mc}), and carbon outputs via burial of organic carbon (F_{bg}) and burial of inorganic carbonates (F_{bc}).

The rate of change of the reservoir of CO_2 in the atmosphere and ocean (A) is:

$$\frac{dA}{dt} = F_{source} - F_{sink} = F_{wg} + F_{wc} + F_{mg} + F_{mc} - F_{bg} - F_{bc} \quad (1)$$

For CO_2 steady state, F_{sink} will be close to F_{source} and $\frac{dA}{dt}$ = 0. Burial of carbonates (F_{bc}) is calculated assuming marine alkalinity balance, i.e. that input from weathering of terrestrial carbonate and silicate rocks will be balanced by total carbonate deposition (19), i.e.

$$F_{bc} = F_{wc} + F_{sil\ weathering} \quad (2)$$

Carbonate weathering (F_{wc}) absorbs one CO_2 molecule for every $CaCO_3$ molecule dissolved, according to the following reversible reaction:

$$CaCO_3 + CO_2 + H_2O \leftrightarrow 2HCO_3^- + Ca^{2+} \quad (3)$$

Calcium carbonate deposition simply reverses the effect of carbonate weathering (eq. 3) and so the carbonate weathering-precipitation cycle is a CO_2 neutral process on long time-scales; this is highlighted by the dashed lines in Figure 2 (see manuscript). This means that the remaining 'net' CO_2 sources must be completely balanced by the two 'net' carbon sinks, which are: organic carbon burial and carbonate deposition following Ca-Mg-silicate weathering. Therefore, the stability of the atmosphere and ocean carbon reservoir over geological timescales is determined by:

$$\frac{dA}{dt} = (F_{wg} + F_{mg} + F_{mc}) - (F_{bg} + F_{sil\ weathering}) \quad (4)$$

The carbonate weathering flux, and the rate of carbonate deposition following carbonate weathering, are not required for the standard calculation of carbon cycle stability. But these fluxes are essential when considering changes in $\delta^{13}C$ – the isotopic signature of carbon liberated during the weathering of carbonates is controlled by the crustal value, whilst the signature of buried carbonates reflects the value in the surface system. Therefore, these terms cannot be removed from the equation governing the change to atmosphere and ocean $\delta^{13}C$.

Low-temperature alteration of the ocean crust is an additional net carbon sink, with increased importance in early Earth history (50), but because it does not impart an isotopic fractionation it may be absorbed into the silicate weathering term without significantly altering our analysis.

The net carbon fluxes drive climate, but the gross fluxes (i.e. including the carbonate weathering-deposition cycle) control $\delta^{13}C$. Moreover, these gross fluxes may potentially have changed by an order of magnitude over the Phanerozoic (due to erosion rate changes – see manuscript) without significantly impacting our picture of the net changes in global carbon cycling and, by extension, climate. Current isotope mass balance models (5, 51) correctly base their $\delta^{13}C$ inversion on the changing gross carbon cycle fluxes, but their analysis assumes that erosion rates do not affect the rate of carbonate weathering, and that rates of erosion over the Phanerozoic have followed a simple cubic trajectory and remained within 0.5 – 1 times the present day rate (44). Implicit in their analysis is therefore the assumption that gross carbon fluxes have remained similar to the present day, and that $\delta^{13}C$ changes must then reflect a change in the net fluxes. For this reason, the predicted rates of organic carbon burial (and

oxygen release) in all previous isotope mass balance studies have closely followed the measured variations in carbonate $\delta^{13}C$.

Carbon cycle modelling

We develop a simple carbon cycle model to test the effects of changes to net and gross carbon fluxes. This model incorporates the temperature dependence of weathering rates and the recycling of crustal material, and is essentially a reduced version of the GEOCARB and COPSE models (19, 5, 6) which considers only the carbon cycle and its variation around the present day steady state. The model code is included here for use with Matlab.

A) Flux calculations

Each flux in the model is defined by a present day rate, *F(0)*, and a set of multipliers that define dependence of the relative rate on other model variables. This follows the approaches used in the most common biogeochemical box models for Phanerozoic climate.

Carbonate and Silicate weathering (F_{wc} and $F_{sil\ weathering}$) are assumed to have a temperature dependence as described in the GEOCARB models (19, 26, 5), with the linear functional form for relative river runoff rate approximated with an exponential (52), to avoid nonphysical negative values when temperature is very low. Dependence of weathering rates on the relative erosion rate (*U*) follows (53), with a weaker dependence for silicate weathering, as observed in field studies (25). The dependence of carbonate weathering rate on the crustal carbonate inventory, *C*, follows the COPSE model (6). Here *T* is temperature in Kelvin.

$$F_{wc} = F_{wc}(0) \times U^{0.9} \times \frac{C}{C(0)} \times e^{0.05(T-288)} \quad (5)$$

$$F_{sil\ weathering} = F_{sil\ weathering}(0) \times U^{0.33} \times e^{7537.69\frac{T-288}{288T}} \times (e^{0.03(T-288)})^{0.65} \quad (6)$$

Weathering of organic carbon (F_{wg}) depends on the relative uplift/erosion rate U, and on the relative abundance of organic carbon in the crust (G). Degassing of organic carbon (F_{mg}), and degassing of carbonates (F_{mc}) are assumed to depend on the crustal inventories of these species, and the material subduction rate, termed D. These follow COPSE (6).

$$F_{wg} = F_{wg}(0) \times U^{0.9} \times \frac{G}{G(0)} \quad (7)$$

$$F_{mg} = F_{mg}(0) \times D \times \frac{G}{G(0)} \quad (8)$$

$$F_{mc} = F_{mc}(0) \times D \times \frac{C}{C(0)} \quad (9)$$

Burial of organic carbon follows the COPSE model, wherein carbon burial scales with bulk sedimentation rate, which has a quadratic dependence on phosphate-limited primary production (6, 31, 54).

$$F_{bg} = F_{bg}(0) \times \left(\frac{P}{P(0)}\right)^2 \quad (10)$$

Burial of carbonates follows equation (2) above.

B) Phosphorus delivery and burial

Following the COPSE model, it is assumed that phosphorus input from weathering is related to the relative rates of silicate, carbonate and organic C weathering.

$$F_{Pinput} = F_{Pinput}(0) \times OB \times \left(\%sil \left(\frac{F_{sil\,weathering}}{F_{sil\,weathering}(0)} \right) + \%carb \left(\frac{F_{wc}}{F_{wc}(0)} \right) + \%org \left(\frac{F_{wg}}{F_{wg}(0)} \right) \right) \quad (11)$$

Here *%sil*, *%carb* and *%org* are the fractions of present day P weathering from each rock type. *OB* is an arbitrary enhancement of P weathering used to test increased organic C burial. Based on the size of each rock reservoir, the COPSE model assumed that $\%sil = \frac{2}{12}, \%carb = \frac{5}{12}, \%org = \frac{5}{12}$. Hartmann et al. (29, 55) estimate P fluxes directly, and show total P release of ~2.7×10^{10} mol/yr from silicate weathering, and ~1×10^{10} mol/yr from carbonates. The organically-derived P flux is difficult to measure, and Compton et al. (30) give ~1.3×10^{10} mol/yr as a maximum. The COPSE model assumes that total P delivery is 4.35×10^{10} mol/yr, which would indicate organic P input of 0.65×10^{10} mol/yr, when taking silicate and carbonate weathering into account. For this work we set organic P delivery at 1×10^{10} mol/yr, as a compromise between these estimates. This gives a total P input of 4.7×10^{10} mol/yr, and sets $\%sil = 0.58, \%carb = 0.21, \%org = 0.21$. We test the model using both these newly-derived P fluxes and the original COPSE input fractions.

The COPSE model calculates P burial via organic, calcium-bound and iron-sorbed forms. 86% of the combined burial flux is through the organic and Ca-bound routes, which are both linked linearly to organic C burial (6). The Fe-bound P burial flux has a complex relationship to ocean anoxia, which is difficult to represent in a non-dimensional model and is beyond the scope of the current study, we therefore simplify the burial function to be a single term, dependent on organic C burial rate.

$$F_{poutput} = F_{poutput}(0) \times \left(\frac{F_{bg}}{F_{bg}(0)} \right) \quad (12)$$

The organic C burial and P cycling in the model is a simplified system based on the dynamics of the marine system, but intended to represent the biosphere as a whole. The qualitative relationship between total P weathering and organic C burial over long timescales is not altered by the evolving land biosphere (6), but additional complexities and feedbacks may affect the quantitative dynamics – potentially resulting in the strengthening or weakening of the relationship between erosion and $\delta^{13}C$ values at different points in Earth history.

C) Reservoir calculations

Total atmosphere and ocean carbon, *A*, is calculated following equation (1). The crustal reservoirs of oxidised carbonate (C) and reduced organic carbon (G) are calculated by summing their respective sources and sinks.

$$\frac{dA}{dt} = F_{wg} + F_{wc} + F_{mg} + F_{mc} - F_{bg} - F_{bc} \quad (13)$$

$$\frac{dG}{dt} = F_{bg} - F_{wg} - F_{mg} \quad (14)$$

$$\frac{dC}{dt} = F_{bc} - F_{wc} - F_{mc} \quad (15)$$

$$\frac{dP}{dt} = F_{pinput} - F_{poutput} \quad (16)$$

In order to track the isotope composition of each reservoir (δR, its $\delta^{13}C$ value), the quantity $R \times \delta R$ is calculated for each reservoir *R*. $\delta^{13}C$ is then calculated by dividing the $R \times \delta R$ value by the size of the reservoir.

$$\frac{d(A\delta A)}{dt} = F_{wg} \times \delta G + F_{wc} \times \delta C + F_{mg} \times \delta G + F_{mc} \times \delta C$$

$$-F_{bg} \times (\delta A - \Delta B) - F_{bc} \times \delta A \quad (17)$$

$$\frac{d(G \times \delta G)}{dt} = F_{bg} \times (\delta A - \Delta B) - F_{wg} \times \delta G - F_{mg} \times \delta G \quad (18)$$

$$\frac{d(C\times\delta C)}{dt} = F_{bc} \times \delta A - F_{wc} \times \delta C - F_{mc} \times \delta C \quad (19)$$

The above equations show the importance of changes in carbonate weathering for calculation of $\delta^{13}C$ values: although the identity $F_{bc} = F_{wc} + F_{sil\ weathering}$ can be used to cancel out F_{wc} in equation (11), the same cannot be applied to equation (14) due to the difference in isotopic compositions.

D) Parameter values and rapid recycling

Size of reservoirs at present day follows GEOCARB (19, 5) and COPSE (6), considering only the 'young' rock reservoirs for *C* and *G*, which constitute the vast majority of interaction with the surface system, and are approximately 10% of the total carbon inventory. This setup mimics the 'rapid recycling' model of (7), which is applied in current GEOCARB modelling (51). In rapid recycling, the larger, ancient rock reservoirs are assumed to remain constant in size, and are therefore omitted from the analysis. The key feature of rapid recycling is that isotopic signatures recorded in young sediments are more quickly recycled to the surface system through weathering. Therefore, atmosphere/ocean $\delta^{13}C$ responds more quickly to changes in carbon fluxes (see manuscript figure 4), but eventually reaches the same steady state. Rapid recycling is removed from the model by increasing the sizes of the modelled crustal organic carbon (*G*) and carbonate carbon (*C*) pools by a factor of 10, to represent the entire reservoir. i.e. replacing equation 21 and 22 with 21* and 22*.

$$A(0) = 3.193 \times 10^{18} \text{ mol} \quad (20)$$

$$G(0) = 1.25 \times 10^{20} \text{ mol} \quad \text{(rapid recycling)} \quad (21)$$

$$C(0) = 5 \times 10^{20} \text{ mol} \quad \text{(rapid recycling)} \quad (22)$$

$$G(0) = 1.25 \times 10^{21} \text{ mol} \quad \text{(no rapid recycling)} \quad (21^*)$$

$$C(0) = 5 \times 10^{21} \text{ mol} \quad \text{(no rapid recycling)} \quad (22^*)$$

217 $P(0) = 3.1 \times 10^{15}$ mol P (23)

218 $\delta A(0) = 0$ ‰ (24)

219 $\delta G(0) = -27$ ‰ (25)

220 $\delta C(0) = 0$ ‰ (26)

221

222 The magnitude of present day carbon fluxes is taken from an assessment of the current
223 literature, taking average values (see manuscript).

224

225 $F_{bg}(0) = 9 \times 10^{12}$ mol yr^{-1} (27)

226 $F_{wg}(0) = 7.75 \times 10^{12}$ mol yr^{-1} (28)

227 $F_{mg}(0) = 1.25 \times 10^{12}$ mol yr^{-1} (29)

228 $F_{wc}(0) = 24 \times 10^{12}$ mol yr^{-1} (30)

229 $F_{mc}(0) = 8 \times 10^{12}$ mol yr^{-1} (31)

230 $F_{sil\ weathering}(0) = 8 \times 10^{12}$ mol yr^{-1} (32)

231 P outputs are assumed to equal inputs at the present day (pre-industrial).

232 $F_{pinput}(0) = 4.7 \times 10^{10}$ mol yr^{-1} (33)

233 $F_{poutput}(0) = 4.7 \times 10^{10}$ mol yr^{-1} (34)

234

235 E) Temperature approximation

236 The CO_2 and temperature approximation follows (56), as in the COPSE model (6). This
237 calculation takes into account the solar insolation (fixed here), atmospheric pCO_2, and a
238 dynamic albedo function. A small correction, *tempcorrect*, is made to give T(0)=288K, as in
239 COPSE, and average surface temperature is calculated from the black body equation, where σ
240 is the Stefan-Boltzmann constant.

241

$$pCO_2 = \frac{A}{A(0)} \times 280 \times 10^{-6} \quad (35)$$

$$\text{SOLAR} = 1368 \text{ W m}^{-2} \quad (36)$$

$$\text{ALBEDO} = 1.4891 - 0.0065979 \times \text{T} + (8.567 \times 10^{-6})T^2 \quad (37)$$

$$tempcorrect = 0.194 \quad (38)$$

$$\sigma = 5.67 \times 10^{-8} \quad \text{W m}^{-2}\ \text{K}^{-4} \quad (39)$$

$$T_{CO2} = 815.17 + (4.895 \times 10^7)T^{-2} - (3.9787 \times 10^5)T^{-1}$$
$$-6.7084(\log(\text{CO2atm}))^{-2} + 73.221(\log(\text{CO2atm}))^{-1}$$
$$-30882T^{-1}(\log(\text{CO2atm}))^{-1} \quad (40)$$

$$T = \left(\frac{SOLAR(1-ALBEDO)}{4\sigma}\right)^{1/4} + T_{CO2} + tempcorrect \quad (41)$$

F) Model code

The attached model code consists of two Matlab scripts: solver.m and equations.m. To run the model, run the solver script in Matlab. Modifications to the model may require alteration of either script, but the scenarios explored in this paper require only modification of the solver script. A 'user panel' is defined at the beginning of the solver script, containing all of the values that must be changed to create the output for this work. Output figures are generated automatically but these and any workspace data must be saved manually if required. The model uses the Matlab ODE solver suite for 'stiff' systems (ODE15s).

Full model output

Figures S3 to S6 show complete model output for the scenarios explored in the manuscript. Figures S3 shows the full model output for ms Figure 3. Figure S4 shows the sensitivity to rapid recycling, under the Hartmann at al. (29) P inputs. Figure S5 shows the full model output for ms Figure 4 (A-D): Carbon isotope excursion driven by an organic C burial event. Figure

S6 shows the full model output for ms Figure 4 (E-H): Carbon isotope excursion driven by an erosion rate change.

A) Effect of an additional direct link between global erosion rates and organic carbon burial.

Whilst sedimentation rates (and therefore organic C burial rates) appear to correlate with primary production (31), it is possible that a global increase in erosion rates may enhance organic carbon burial by a greater factor than is considered in our model through additional preservation effects (5). We explore this idea by giving the rate of organic C burial an additional direct dependence on the global uplift/erosion rate in figure S4. Aside from the concentration of ocean phosphate (shown in magenta), the steady state results are unchanged and plot over the original model runs. This is because increased preservation of organic carbon results in an increased phosphate sink, which is self-limiting. The organic C burial rate in our model adjusts so that the amount of phosphate buried is equal to the phosphate input, which is unchanged in the new scenario.

This discussion is by no means complete, and the drivers of organic C burial rates at the global scale remain complex and incompletely understood. But as we note in the manuscript, a strong link between the global erosion rate and the rate of organic C burial is effectively falsified by the anti-correlation between carbonate $\delta^{13}C$ and erosion/sedimentation proxies.

B) Effect of fixing the $\delta^{13}C$ value of carbon inputs.

Figure S7 shows the same scenario as figure S6, but with the isotopic value of carbon inputs ($\delta^{13}C_{in}$) fixed at -6‰. Under this assumption (red lines), the response of $\delta^{13}C_{carb}$ to the reduction in erosion rate is reduced by around 1‰, but is qualitatively similar. This confirms that the mechanism we describe in the manuscript does not rely on changes in the $\delta^{13}C$ value of carbon

inputs, although these changes do contribute to the values of $\delta^{13}C_{carb}$ predicted by our model. $\delta^{13}C_{in}$ is affected both by the changes to carbonate and organic carbon weathering fluxes brought about by erosion rate changes, and by the changing isotopic composition of the crustal carbon reservoirs themselves.

Figure legends

Fig. S1. Correlations between carbonate $\delta^{13}C$ and rates of sediment deposition (A), erosion/uplift parameter used in long term models (B) and $^{87}Sr/^{86}Sr$ of seawater. The $\delta^{13}C$ data follows (33), and is averaged over the bins used in the study of (34) for panel A, and over 10 Myr bins for panels B and C.

Fig. S2. Secular trends in key isotopic parameters in zircons and marine carbonates (57, 48, 43). Magmatic zircon abundances reveal when five supercontinents formed through orogenic collision (grey shading above), leading to greatly increased reworking of sediment during magmatism (red arrows mark resultant increases in zircon $\delta^{18}O$). The zircon Hf and seawater Sr isotope records anti-correlate, confirming that the Ediacaran-Ordovician interval was a time of exceptional erosional unroofing of crustal roots (48). The $\delta^{13}C$ (f_{org}) minimum at ~500 Ma (49), shown as a dashed green line, occurred during the peak in Gondwanan orogenesis. $\delta^{13}C$ (f_{org}) maxima (49), shown as dashed red lines, coincide with the existence of Pangea and Rodinia, respectively, before onset of break-up.

Fig. S3. Full model output for ms figure 3 showing steady states for changes in the relative uplift rate. Organic carbon reservoirs and fluxes are coloured red and carbonate reservoirs and fluxes are coloured blue. 'deltaA' denotes the isotopic composition of reservoir A (‰ relative to PDB). As in the manuscript, M1 shows P input ratios derived from (29), M2 shows ratios from COPSE and M3 assumes that P weathering follows the same relationships to uplift and temperature as carbonate weathering.

Fig. S4. Full model output for ms figure 3 showing steady states for changes in the relative uplift rate. This figure shows effect of rapid recycling on steady states: solid lines show RR

on, fainter lines show RR off. Note that surface reservoir steady states are unchanged, but crustal reservoirs now show larger bulk values instead of 'young' values. The figure also shows a scenario in which the rate of organic carbon burial has an additional linear dependency on the relative uplift/erosion rate. This changes only the values for ocean phosphate (shown in magenta).

Fig. S5. Full model output for ms figure 4 A-D (case 1) showing system response over time to an increase in organic C burial rate. Organic carbon reservoirs and fluxes are coloured red and carbonate reservoirs and fluxes are coloured blue. 'deltaA' denotes the isotopic composition of reservoir A (‰ relative to PDB). Green lines show forcing functions for uplift and relative P weathering enhancement.

Fig. S6. Full model output for ms figure 4 E-H (case 2) showing system response over time to a decrease in the uplift/erosion rate. Organic carbon reservoirs and fluxes are coloured red and carbonate reservoirs and fluxes are coloured blue. 'deltaA' denotes the isotopic composition of reservoir A (‰ relative to PDB). Green lines show forcing functions for uplift and relative P weathering enhancement.

Fig. S7. Additional model output for ms figure 4 E-H (case 2) showing system response over time to a decrease in the uplift/erosion rate when the $\delta^{13}C$ value of carbon inputs is fixed at -6‰ (red lines), compared to full model (black lines).

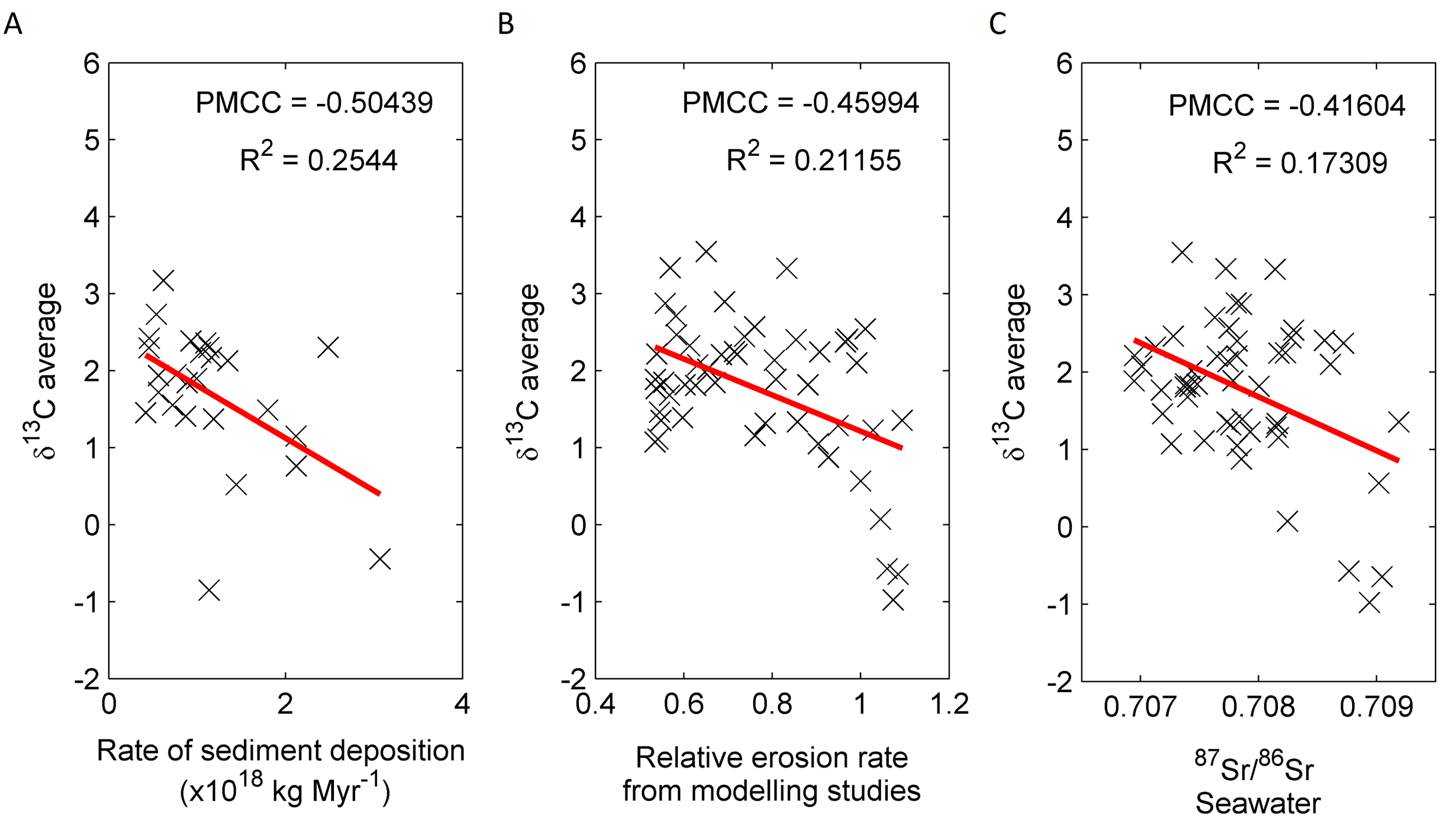
A
PMCC = -0.50439
R2 = 0.2544
δ13C average
Rate of sediment deposition
(x1018 kg Myr-1)
B
PMCC = -0.45994
R2 = 0.21155
δ13C average
Relative erosion rate
from modelling studies
C
PMCC = -0.41604
R2 = 0.17309
δ13C average
87Sr/86Sr
Seawater

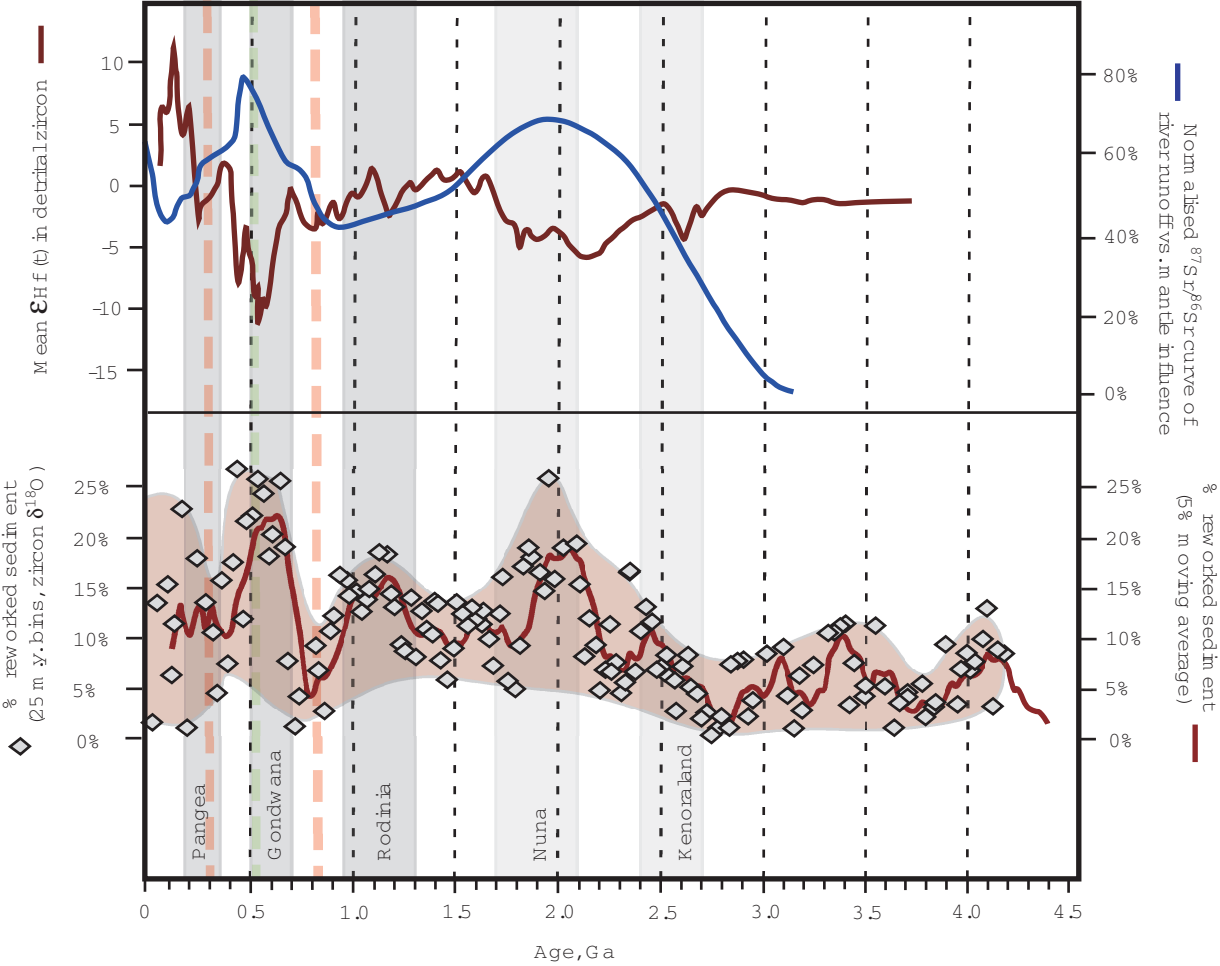
Mean εHf(t) in detrital zircon
Normalised 87Sr/86Sr curve of river runoff vs. mantle influence
% reworked sediment (25 my. bins, zircon δ18O)
% reworked sediment (5% moving average)
10
5
0
-5
-10
-15
80%
60%
40%
20%
0%
25%
20%
15%
10%
5%
0%
Pangea
Gondwana
Rodinia
Nuna
Kenoraland
0
0.5
1.0
1.5
2.0
2.5
3.0
3.5
4.0
4.5
Age, Ga

A

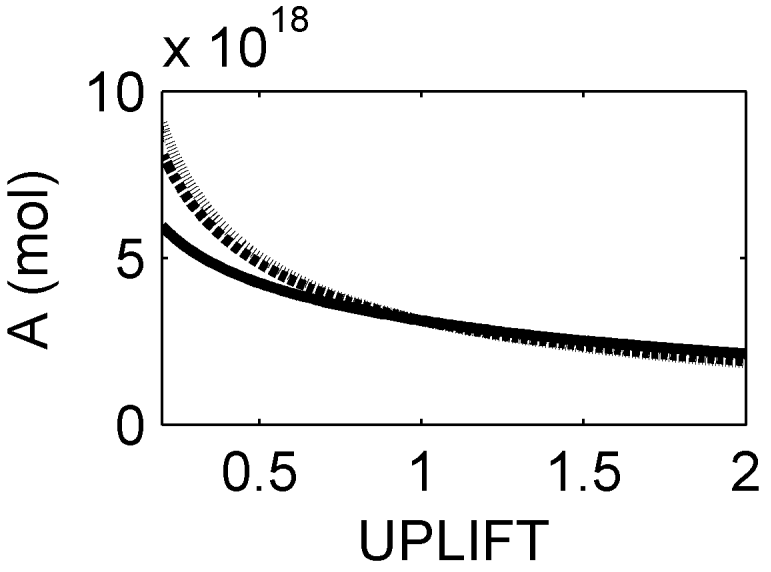
x 10^18
10
5
0
A (mol)
0.5
1
1.5
2
UPLIFT

B

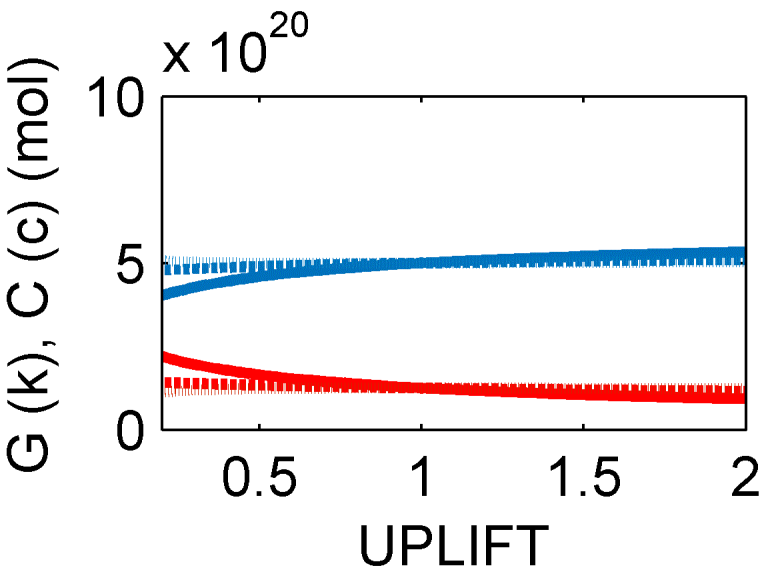
x 10^20
10
5
0
G (k), C (c) (mol)
0.5
1
1.5
2
UPLIFT

C

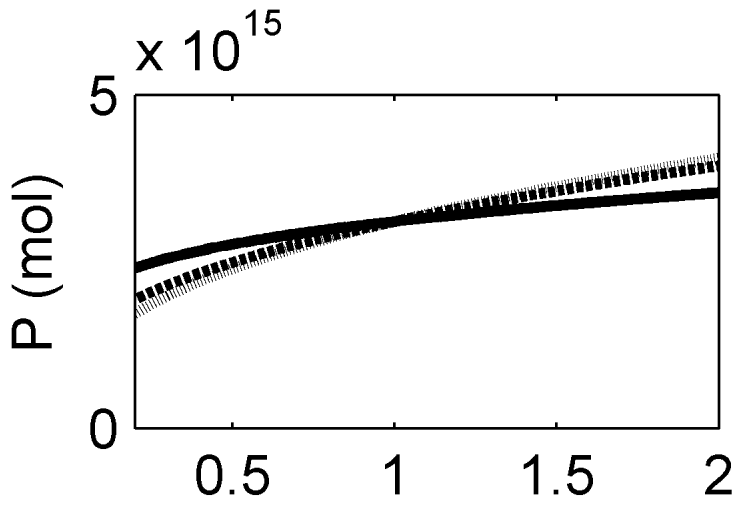
x 10^15
5
0
P (mol)
0.5
1
1.5
2
UPLIFT

D

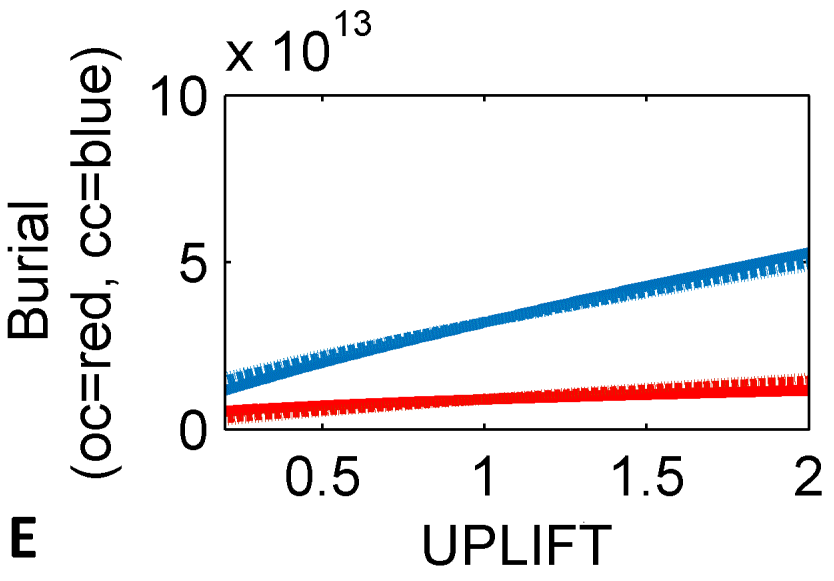
x 10^13
10
5
0
Burial
(oc=red, cc=blue)
0.5
1
1.5
2
UPLIFT

E

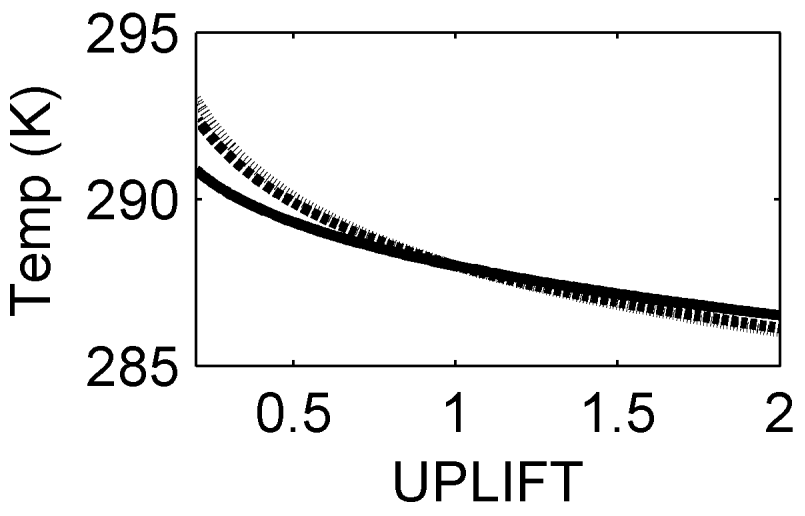
295
290
285
Temp (K)
0.5
1
1.5
2
UPLIFT

F

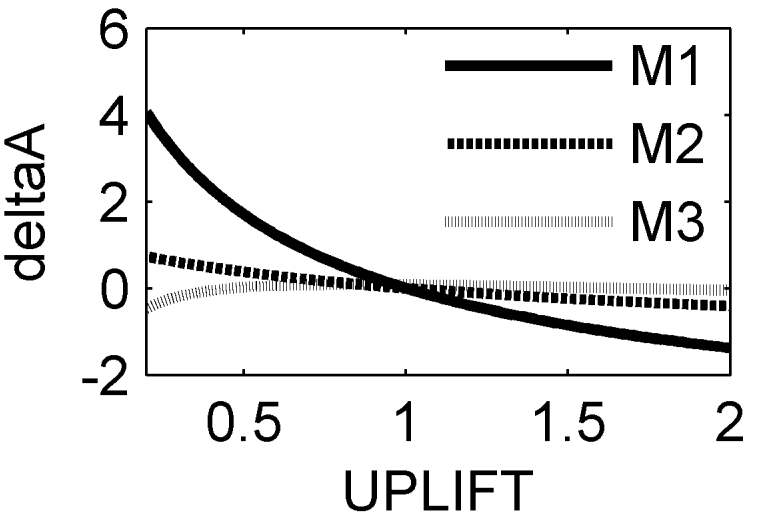
6
4
2
0
-2
deltaA
M1
M2
M3
0.5
1
1.5
2
UPLIFT

G

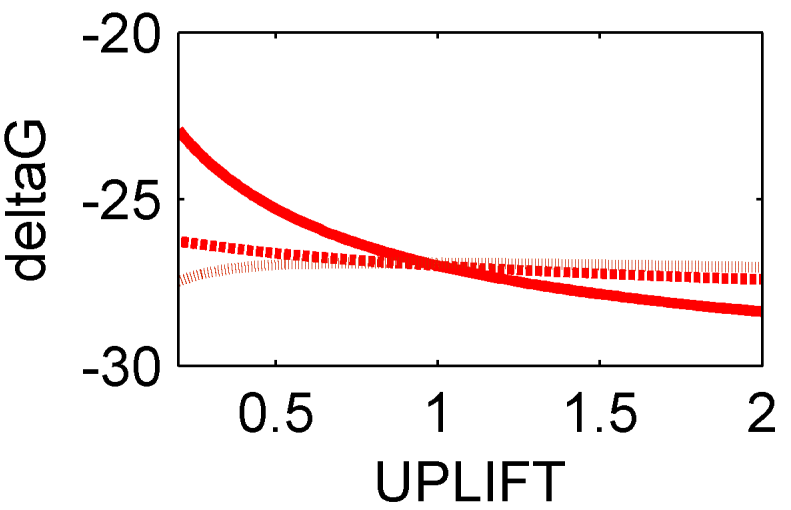
-20
-25
-30
deltaG
0.5
1
1.5
2
UPLIFT

H

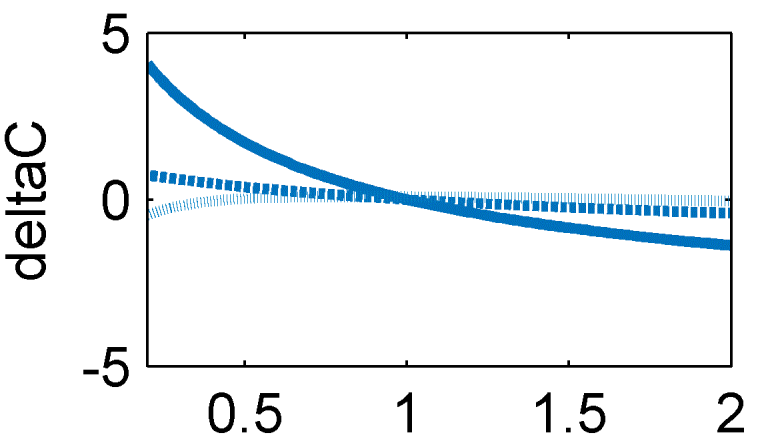
5
0
-5
deltaC
0.5
1
1.5
2
UPLIFT

I

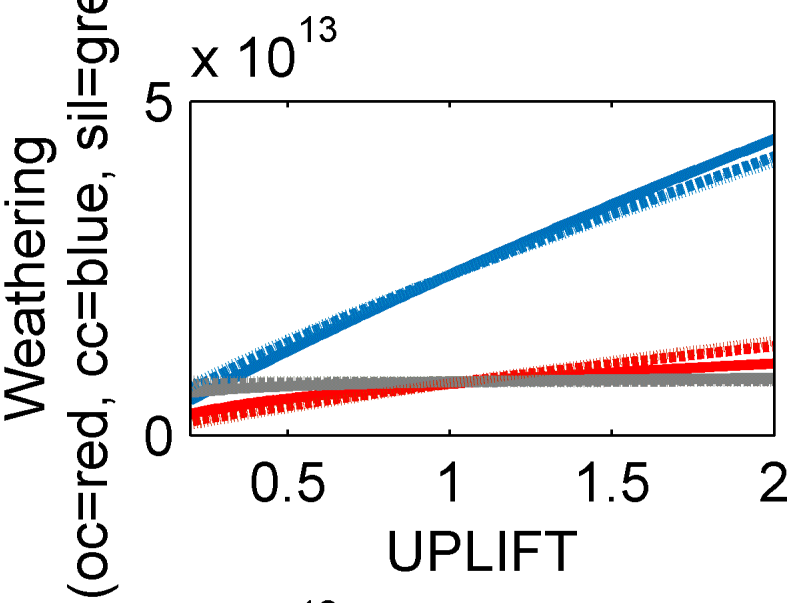
x 10^13
5
0
Weathering
(oc=red, cc=blue, sil=grey)
0.5
1
1.5
2
UPLIFT

J

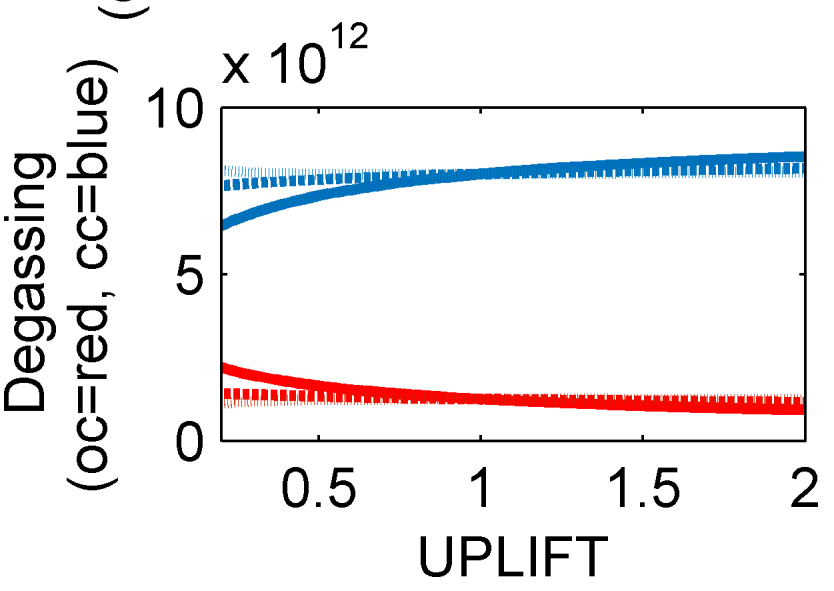
x 10^12
10
5
0
Degassing
(oc=red, cc=blue)
0.5
1
1.5
2
UPLIFT

A

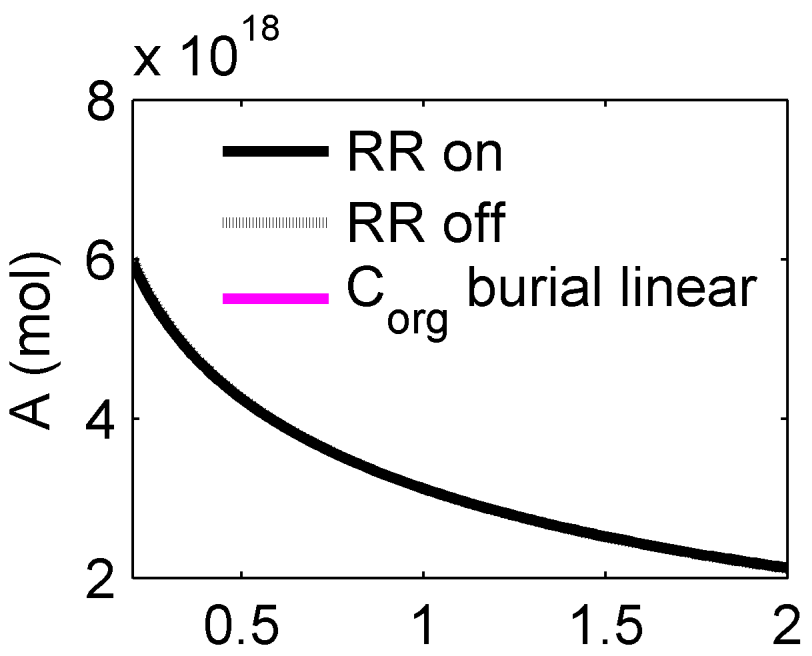
x 10^18
A (mol)
RR on
RR off
C_org burial linear
UPLIFT

B

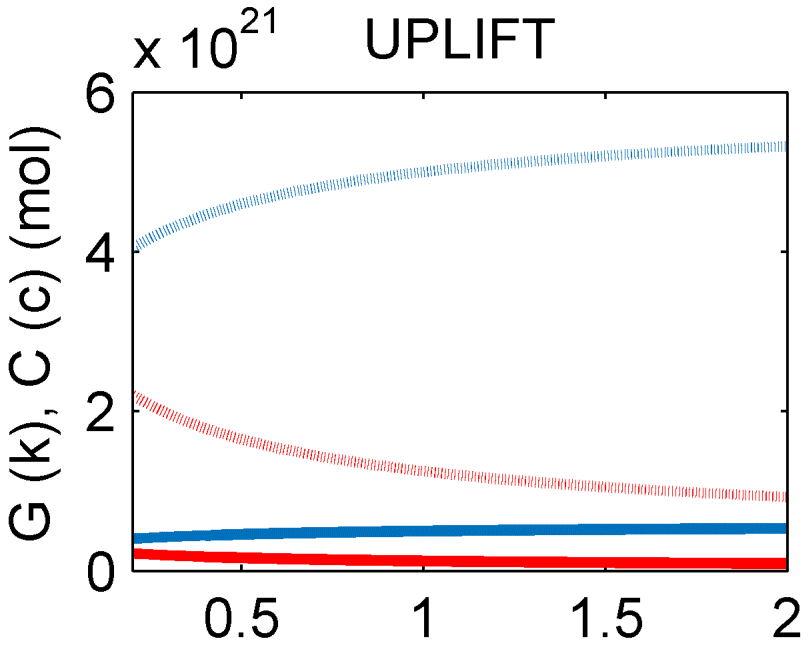
x 10^21
G (k), C (c) (mol)
UPLIFT

C

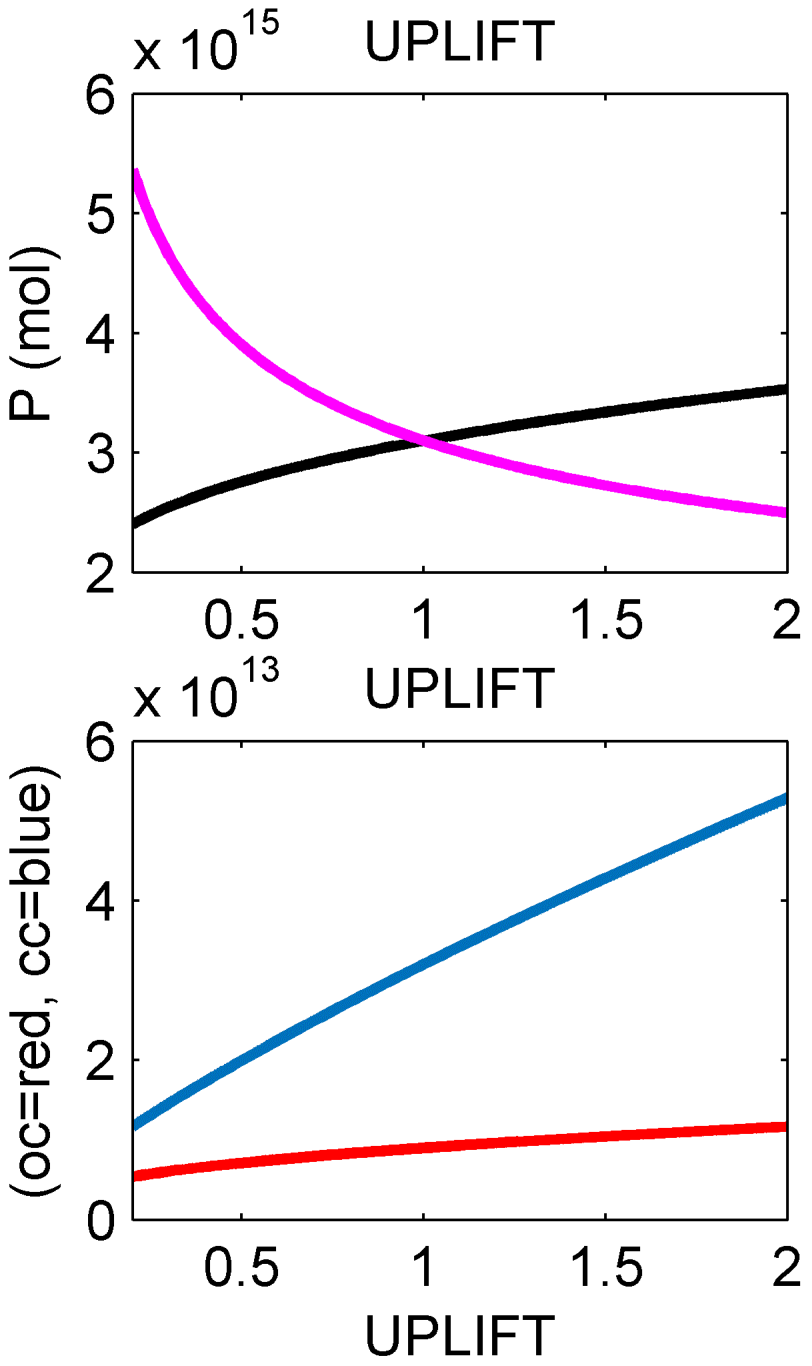
x 10^15
P (mol)
UPLIFT

D

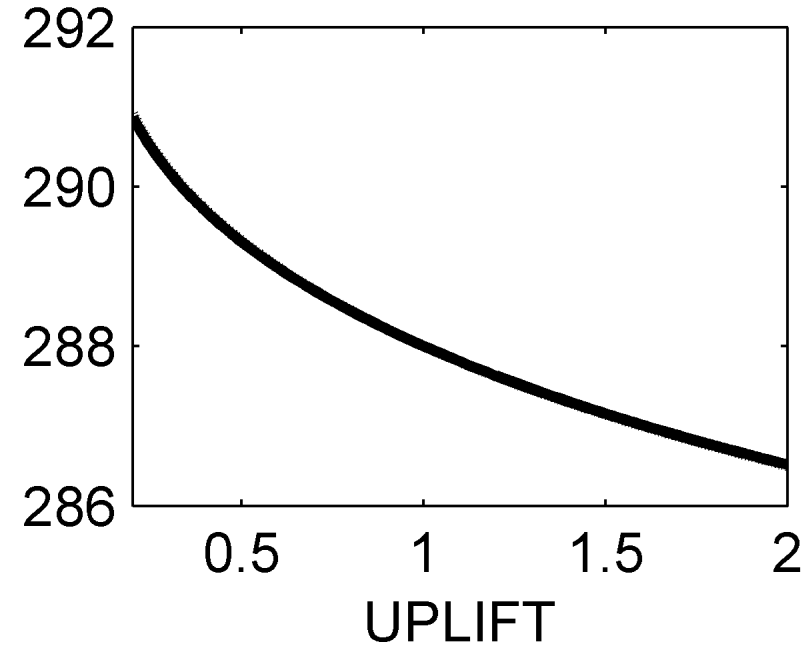
x 10^13
Burial
(oc=red, cc=blue)
UPLIFT

E

Temp (K)
UPLIFT

F

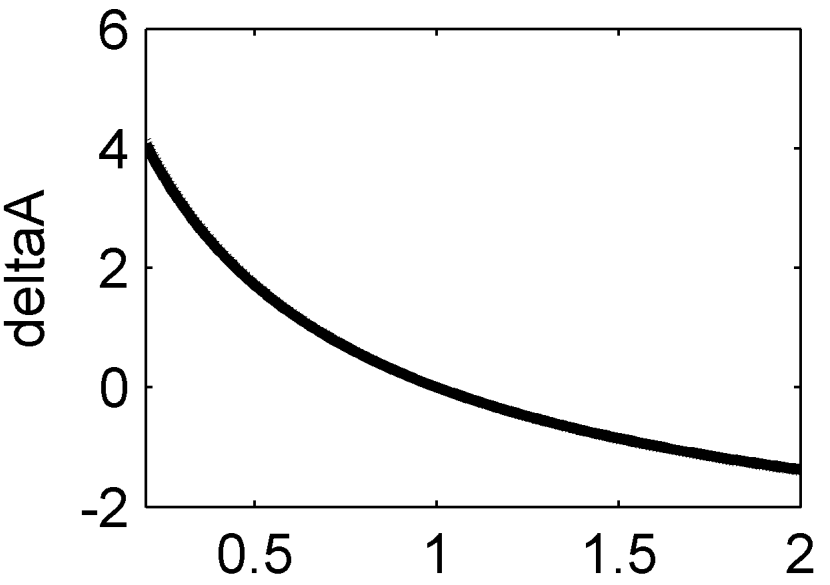
deltaA
UPLIFT

G

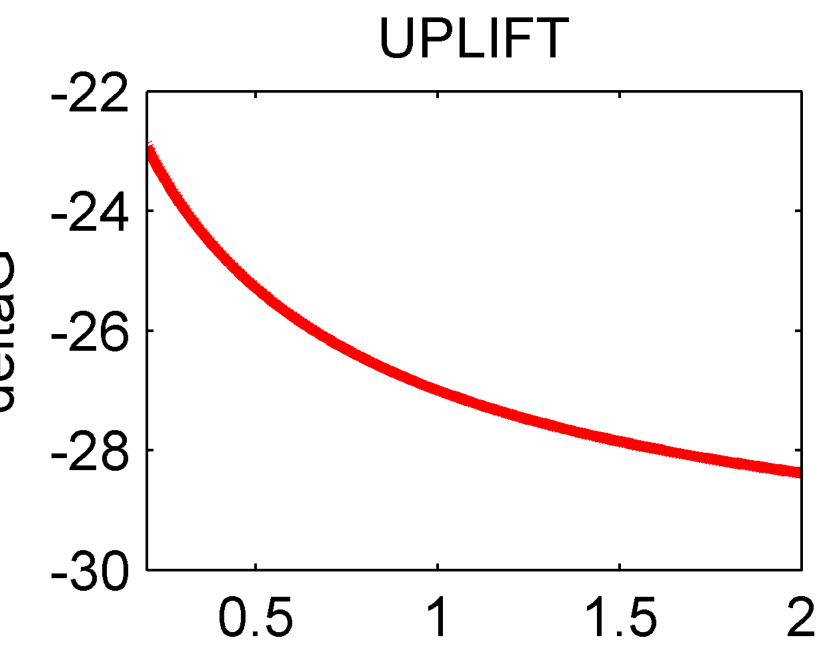
deltaG
UPLIFT

H

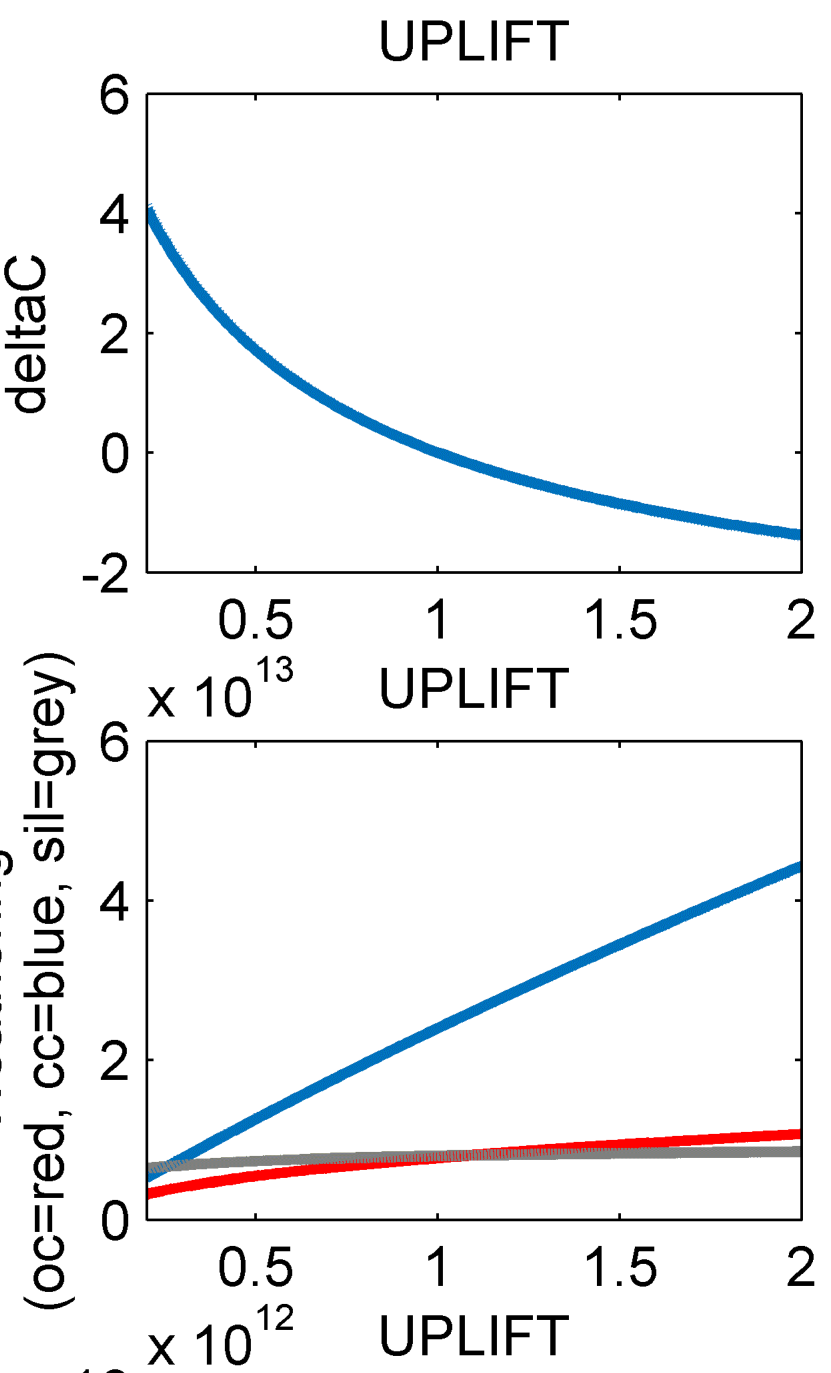
deltaC
UPLIFT

I

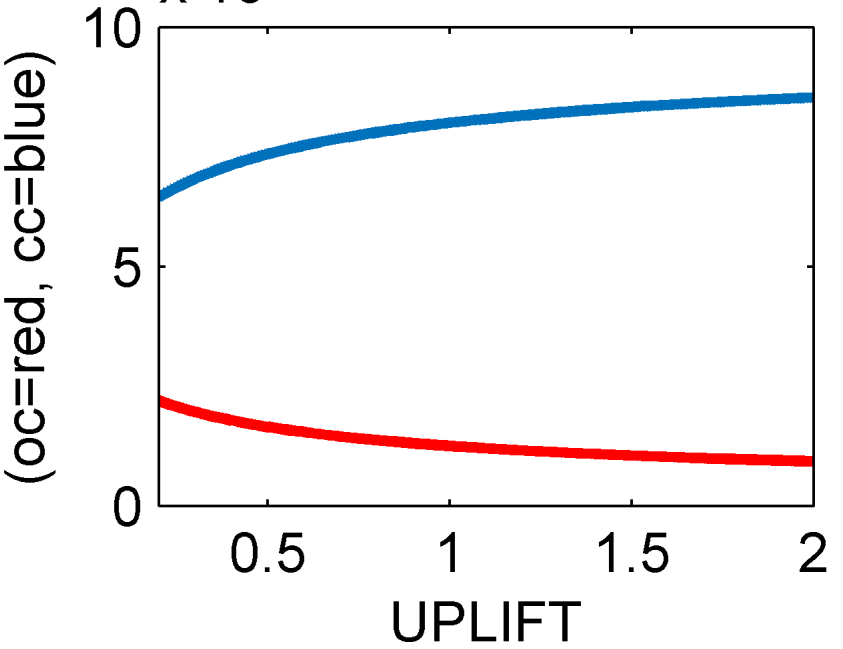
x 10^13
Weathering
(oc=red, cc=blue, sil=grey)
UPLIFT

J

x 10^12
Degassing
(oc=red, cc=blue)
UPLIFT

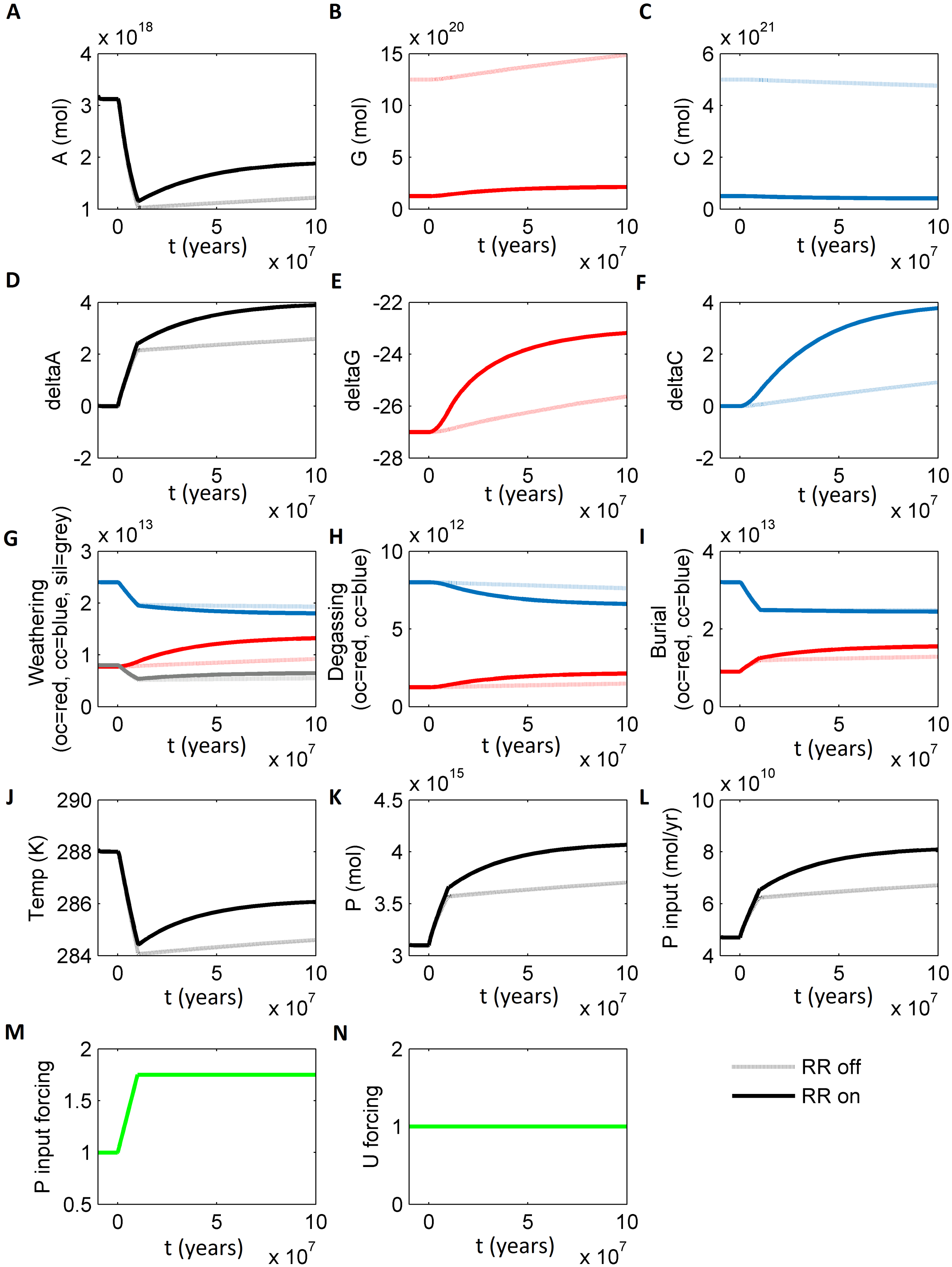
A
x 10^18
A (mol)
t (years)
x 10^7
B
x 10^20
G (mol)
t (years)
x 10^7
C
x 10^21
C (mol)
t (years)
x 10^7
D
deltaA
t (years)
x 10^7
E
deltaG
t (years)
x 10^7
F
deltaC
t (years)
x 10^7
G
x 10^13
Weathering
(oc=red, cc=blue, sil=grey)
t (years)
x 10^7
H
x 10^12
Degassing
(oc=red, cc=blue)
t (years)
x 10^7
I
x 10^13
Burial
(oc=red, cc=blue)
t (years)
x 10^7
J
Temp (K)
t (years)
x 10^7
K
x 10^15
P (mol)
t (years)
x 10^7
L
x 10^10
P input (mol/yr)
t (years)
x 10^7
M
P input forcing
t (years)
x 10^7
N
U forcing
t (years)
x 10^7
RR off
RR on

A

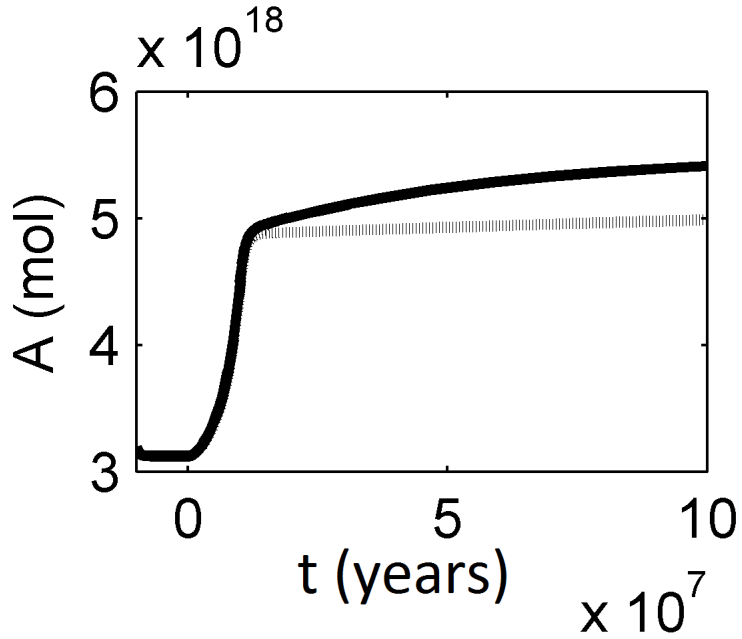

B

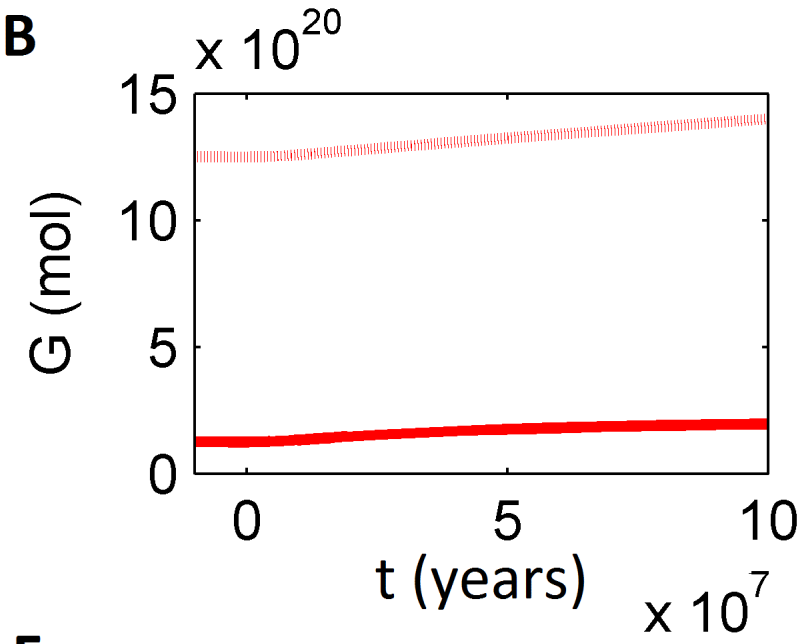

C

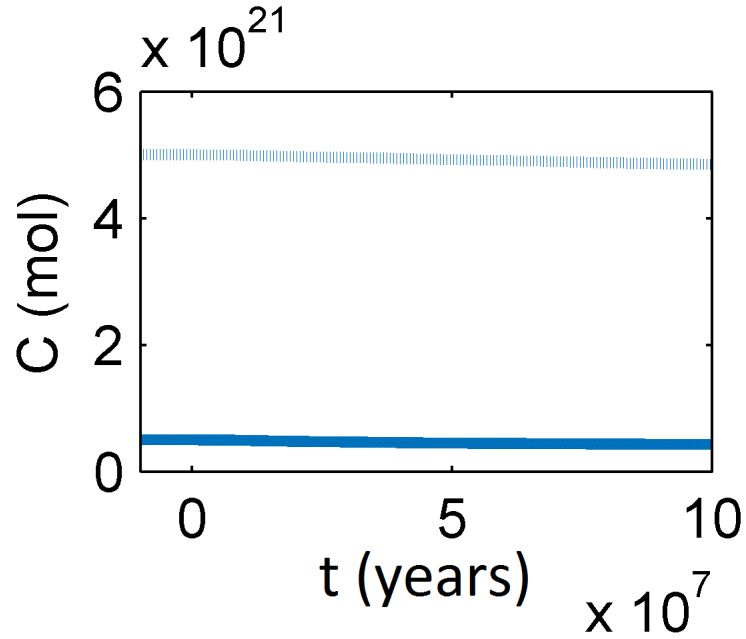

D

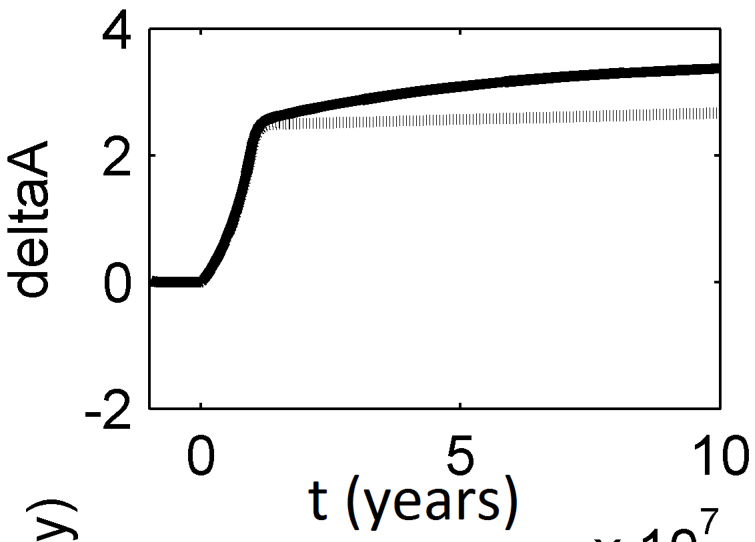

E

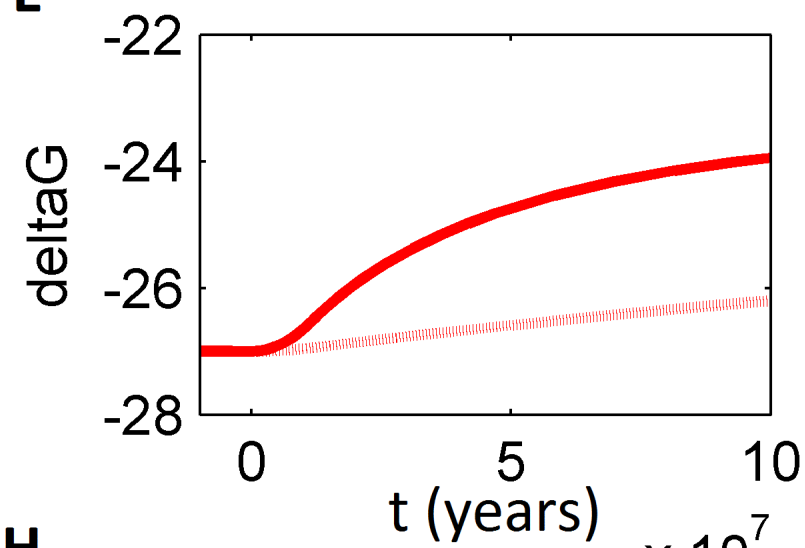

F

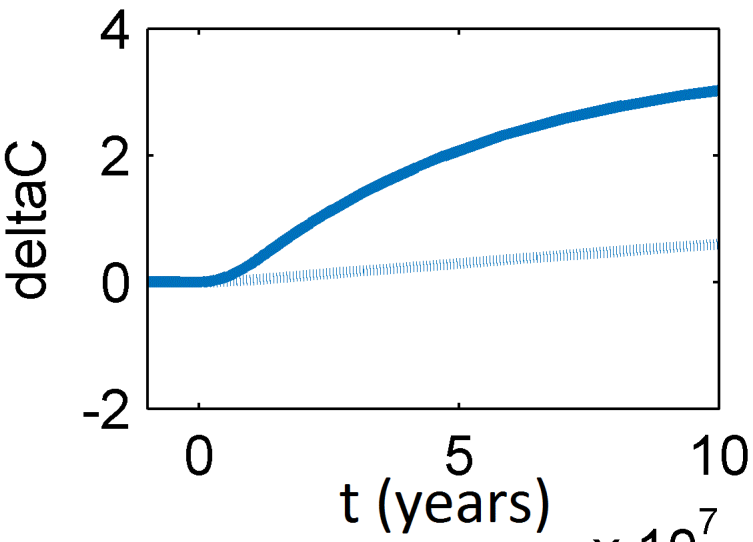

G

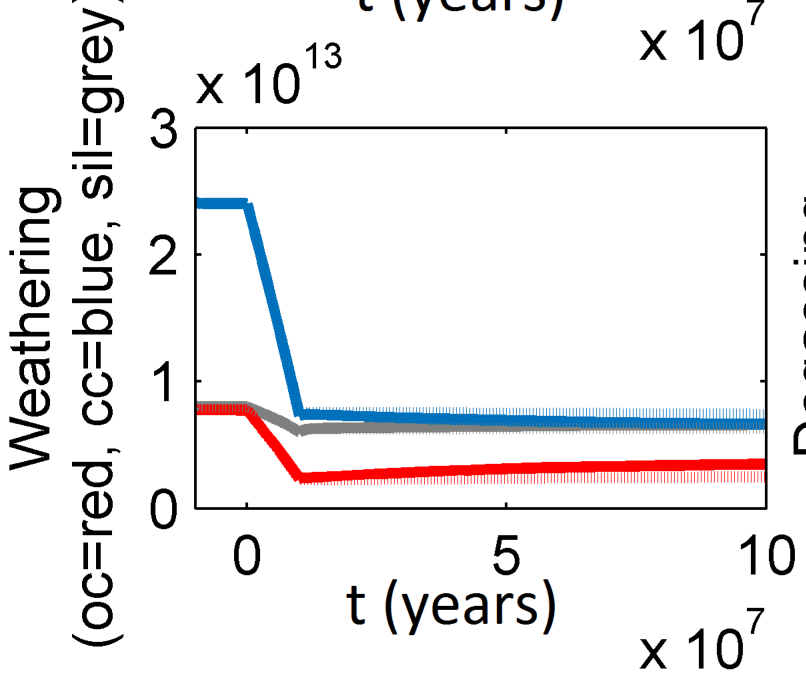

H

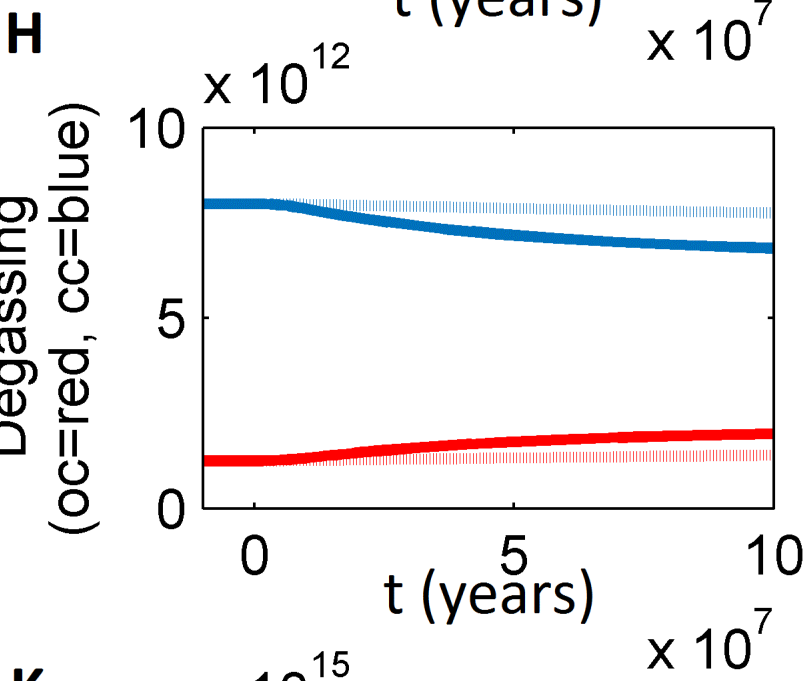

I

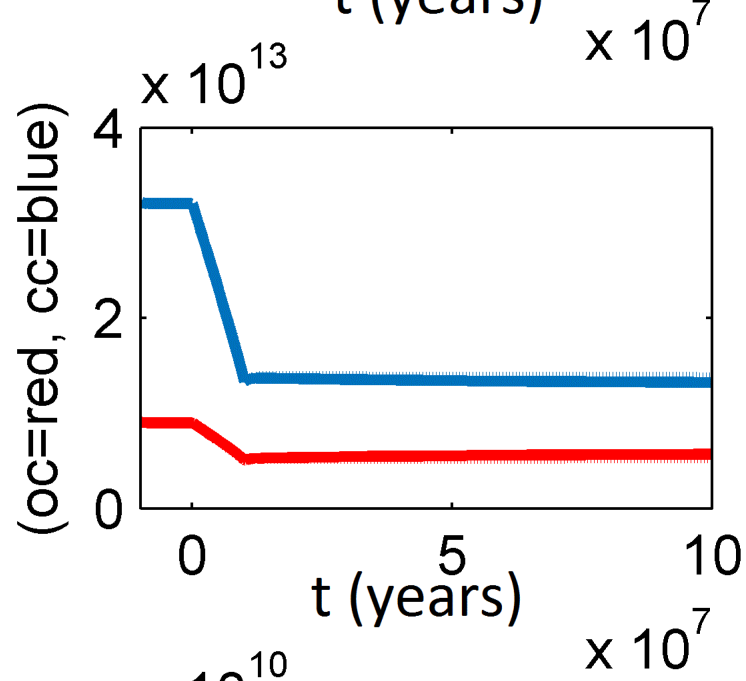

J

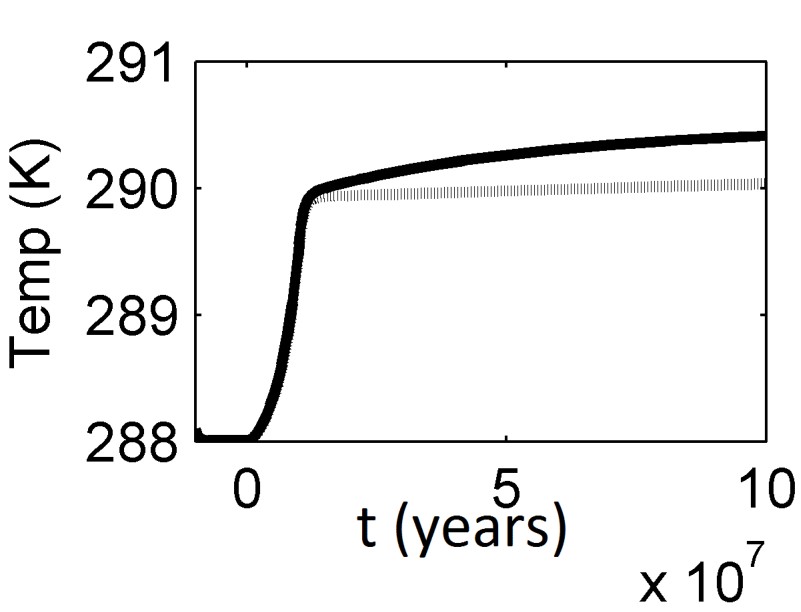

K

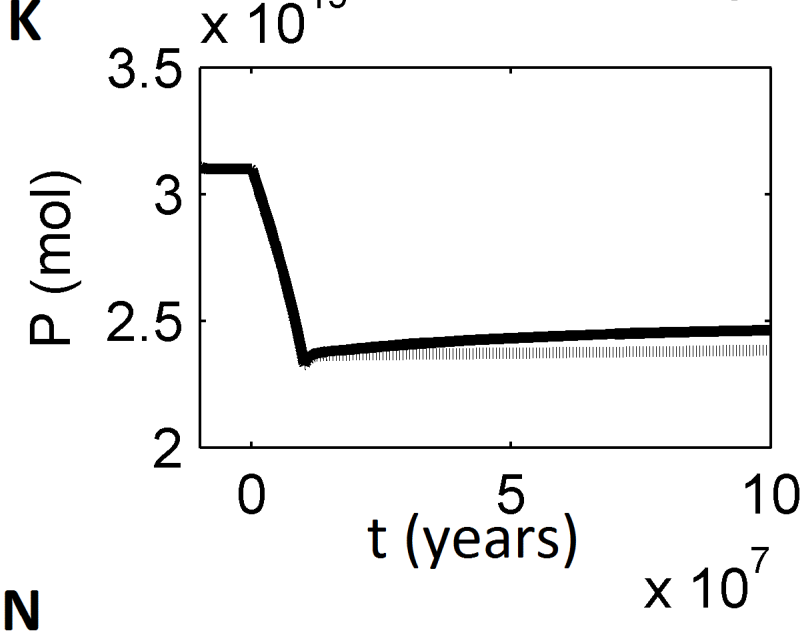

L

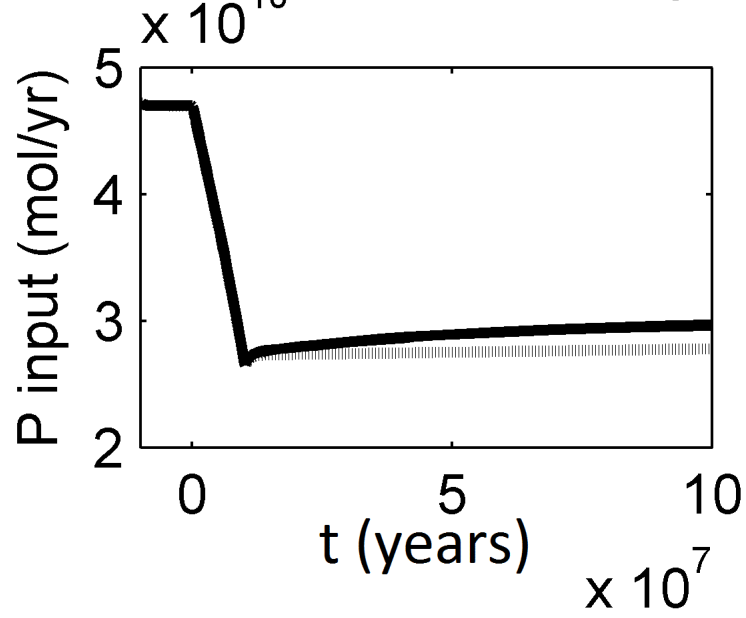

M

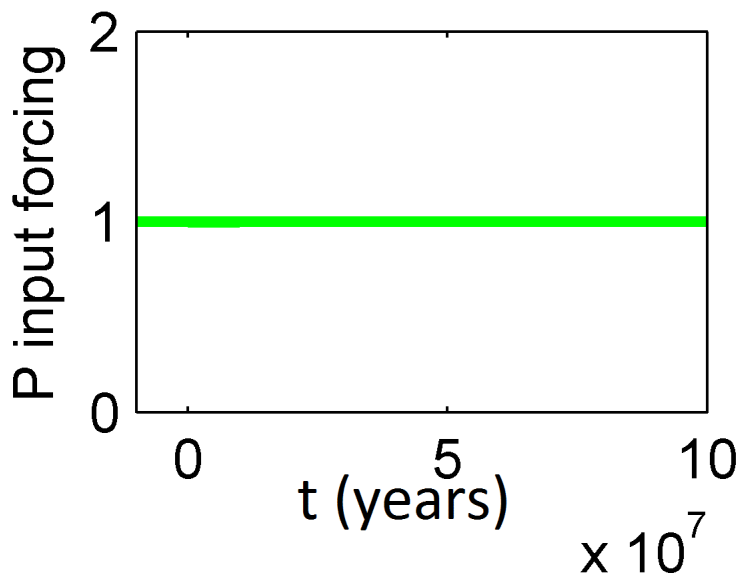

N

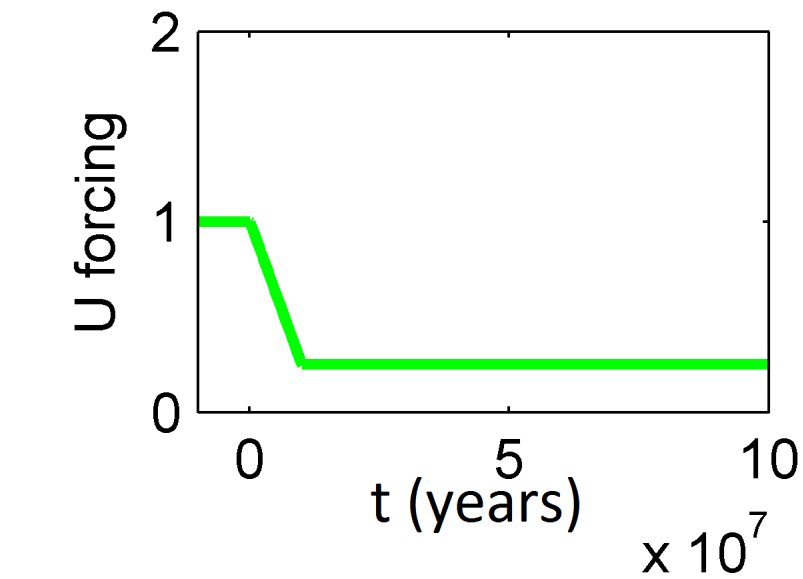

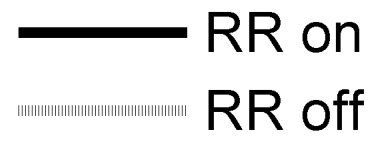

A

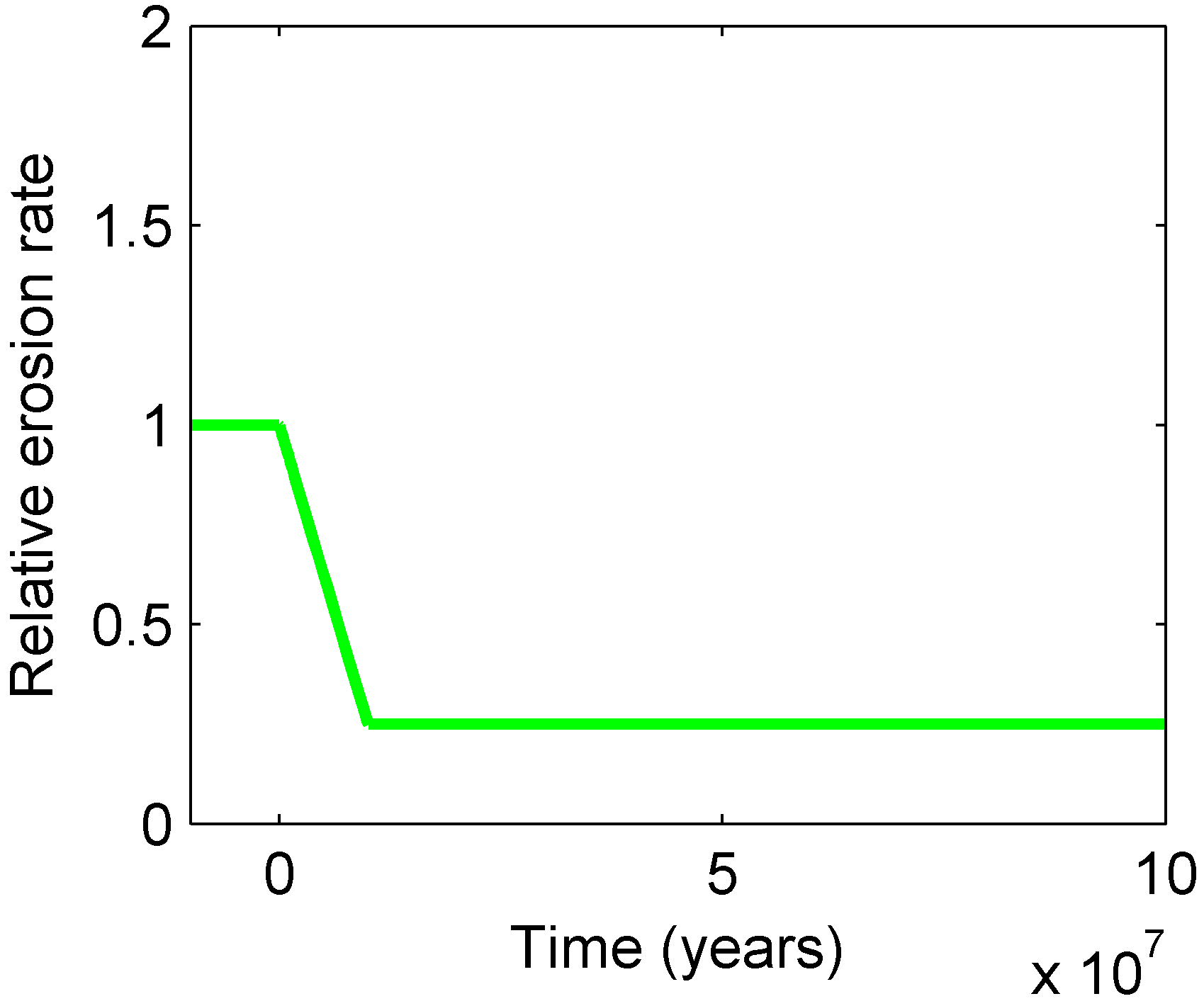
2
1.5
1
0.5
0
Relative erosion rate
0
5
10
Time (years)
x 10^7

B

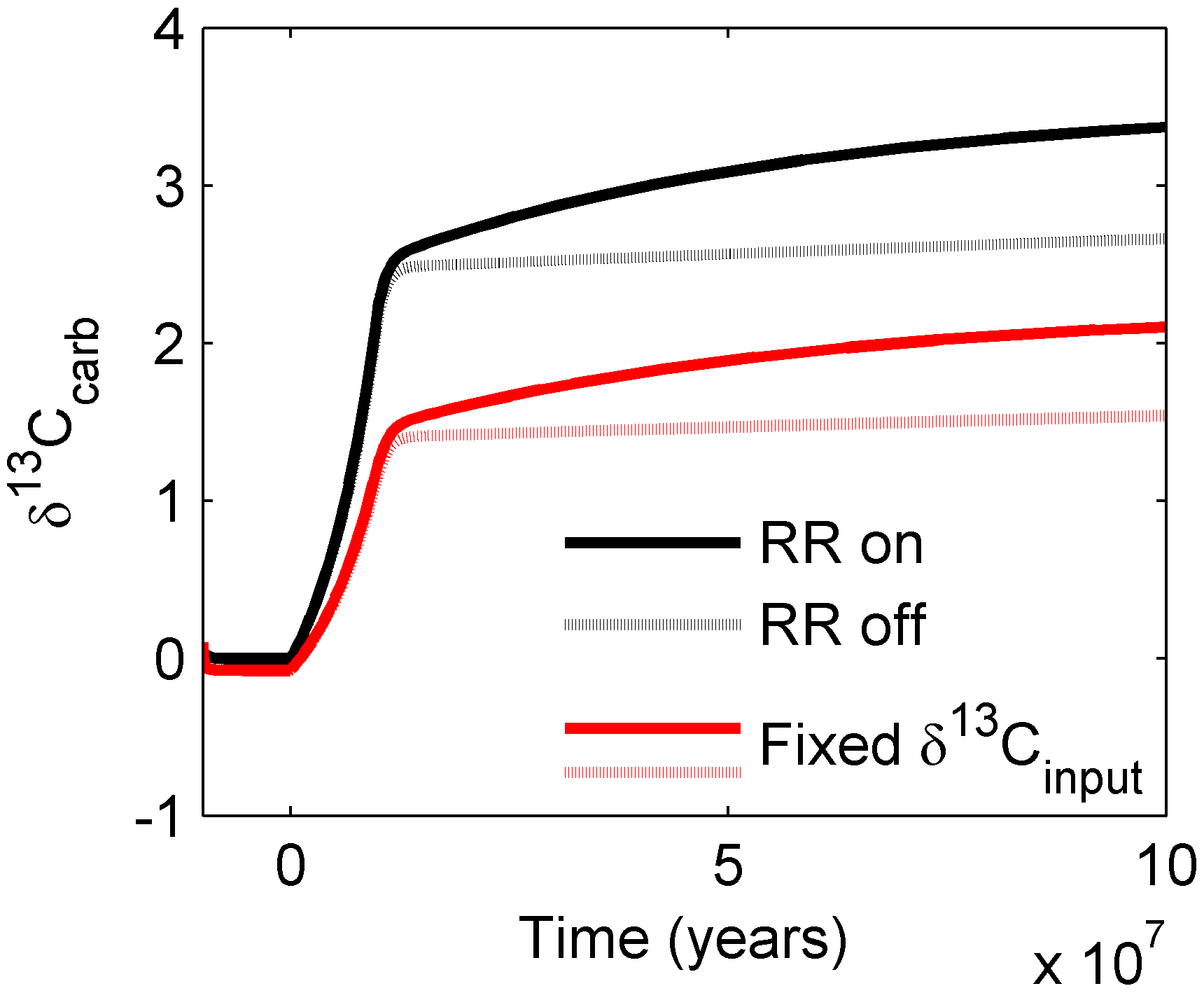
4
3
2
1
0
-1
δ13Ccarb
RR on
RR off
Fixed δ13Cinput
0
5
10
Time (years)
x 10^7